Geochemistry Geophysics Geosystems G3

Article
Volume 12, Number 3
10 March 2011
Q03004, doi:10.1029/2010GC003347
ISSN: 1525-2027

Published by AGU and the Geochemical Society

Seismic interpretation of pelagic sedimentation regimes in the 18–53 Ma eastern equatorial Pacific: Basin-scale sedimentation and infilling of abyssal valleys

Masako Tominaga
Department of Oceanography, Texas A&M University, College Station, Texas 77843, USA

Now at Department of Geology and Geophysics, Woods Hole Oceanographic Institution, Woods Hole, Massachusetts 02543, USA (mtominaga@whoi.edu)

Mitchell Lyle
Department of Oceanography, Texas A&M University, College Station, Texas 77843, USA

Neil C. Mitchell
School of Earth, Atmospheric, and Environmental Sciences, University of Manchester, Manchester M13 9PL, UK

[1] Understanding how pelagic sediment has been eroded, transported, and deposited is critical to evaluating pelagic sediment records for paleoceanography. We use digital seismic reflection data from an Integrated Ocean Drilling Program site survey (AMAT03) to investigate pelagic sedimentation across the eastern-central equatorial Pacific, which represents the first comprehensive record published covering the 18–53 Ma eastern equatorial Pacific. Our goals are to quantify (1) basin-hill-scale primary deposition regimes and (2) the extent to which seafloor topography has been subdued by abyssal valley-filling sediments. The eastern Pacific seafloor consists of a series of abyssal hills and basins, with minor late stage faulting in the basement. Ocean crust rarely outcrops at the seafloor away from the rise crest; both hills and basins are sediment covered. The carbonate compensation depth is identified at 4440 m by the appearance of acoustically transparent clay intervals in the seismic data. Overall, we recognized three different sedimentation regimes: depositional (high sedimentation rate), transitional, and minimal sedimentation (low sedimentation rate) regimes. In all areas, the sedimented seafloor mimics the underlying basement topography, although the degree to which topography becomes subdued varies. Depositional regimes result in symmetric sedimentation within basins and subdued topography, whereas minimal sedimentation regimes have more asymmetric distribution of sediments within topographic lows and higher seafloor relief. Regardless of sedimentation regime, enhanced sediment deposition occurs within basins. However, we observe that basin infill is rarely more than twice as thick as sediment cover over abyssal hills. If this variation is due to sediment focusing, the focusing factor in the basins, as measured by ^{230}Th, is no more than a factor of ~1.3 of the total vertical particulate rain.

Components: 12,600 words, 9 figures, 4 tables.

Keywords: equatorial Pacific; multichannel seismic reflection; Ocean Drilling Program.

Index Terms: 3022 Marine Geology and Geophysics: Marine sediments: processes and transport; 3025 Marine Geology and Geophysics: Marine seismics (0935, 7294); 3036 Marine Geology and Geophysics: Ocean drilling.

Received 26 August 2010; **Revised** 30 December 2010; **Accepted** 4 January 2011; **Published** 10 March 2011.

Tominaga, M., M. Lyle, and N. C. Mitchell (2011), Seismic interpretation of pelagic sedimentation regimes in the 18–53 Ma eastern equatorial Pacific: Basin-scale sedimentation and infilling of abyssal valleys, *Geochem. Geophys. Geosyst.*, *12*, Q03004, doi:10.1029/2010GC003347.

1. Introduction

[2] Understanding the first-order pelagic sedimentation regime is critical to the accurate evaluation of the paleoceanographic record because sedimentation is the recording process for paleoceanographic signals. Sedimentation processes potentially can blur the record if the sediment is transported and mixed over long distances or if the proxies are degraded during diagenesis. Paleoceanographic studies typically assume that sedimentation processes cause minimal distortion of the environmental record. In fact, paleoceanographers often look for basins or drifts that have abnormally high sedimentation rates, in order to extract high-resolution time series [e.g., *Peterson et al.*, 2000; *McManus et al.*, 1999]. Exactly how the sedimentation process records, distorts, and preserves the environmental information is often neglected.

[3] Pelagic and hemipelagic sediments are thought to be deposited by slow vertical sedimentation producing layers of sediment that uniformly drape over the seafloor [*Menard*, 1964]. It has been assumed by marine geologists that pelagic sediments have fallen more or less directly down from the surface ocean in a relatively rapid manner [*McCave*, 1975; *Takahashi and Honjo*, 1981; *Dymond and Lyle*, 1985; *Alldredge and Gotschalk*, 1988], based upon acoustic and seismic surveys made in the 1960s [e.g., *Ewing et al.*, 1964, 1966]. To date, few researchers have studied how sedimentation has affected seafloor topography over time, and their works were limited to near surface data or to narrow geographic regions [e.g., *Laguros and Shipley*, 1989; *Malinverno*, 1990; *Mitchell*, 1995].

[4] Lack of information about the in situ sedimentation regime can lead to major uncertainties in determining the chemical budget in sediments. In recent years there has developed a concern that significant amounts of the sediment in a pelagic deposit does not reflect the surface environment directly above but has arrived through horizontal sediment transport. The sediment deposit thus represents an environmental signal integrated over significant horizontal distances [e.g., *Marcantonio et al.*, 2001; *Francois et al.*, 2004; *Lyle et al.*, 2005; *Francois et al.*, 2007; *Lyle et al.*, 2007]. Much of the evidence for large-scale horizontal sediment transport is based on geochemical measurements and application of simple models to describe the distribution of the geochemical tracers. It is important to critically examine the geochemical sediment models and to compare these data to independent marine geological estimates of sedimentation to understand how sediments are redistributed.

[5] The equatorial Pacific seafloor is covered by a few hundred meters of biogenic sediments [e.g., *Menard*, 1964; *van Andel and Moore*, 1974]. Seafloor crust on the Pacific plate has traveled across the equatorial productivity zone after it was formed at the East Pacific Rise and hence, has received sediments with sedimentation rates that vary over time depending on latitudinal differences in the surface primary productivity and other factors [*Mitchell et al.*, 2003; *Moore et al.*, 2004]. Furthermore, the equatorial Pacific behaves as a common sediment province in which sedimentation events can be tracked over length scales >1000 km [*Mayer et al.*, 1986; *Pälike et al.*, 2005]. This setting makes the subsurface structure of the pelagic sediment blanket unique, so that we can trace important sediment layers millions of years apart over thousands of kilometers [*Mayer et al.*, 1986; *Bloomer et al.*, 1995; *Lyle et al.*, 2002b]. The equatorial Pacific seafloor topography is also simple, characterized by abyssal hills and basins, and is ideal to investigate abyssal-hill-scale sedimentation processes. We can observe how these processes change depending on sedimentation rate from depositional (high sedimentation rate) to minimal sedimentation (low sedimentation rate). Finally, this region is protected from continentally derived turbidites by the East Pacific Rise, which traps these sediments to the east of it.

[6] A few researchers have sought to evaluate whether the diffusion transport model (in which the sediment surface topography obeys a diffusion equation) could represent pelagic sediment deposition on the Mid-Atlantic Ridge [*Webb and Jordan*, 1993; *Mitchell*, 1995; *Webb and Jordan*, 2001a, 2001b]. Those results were somewhat ambiguous as some surfaces are consistent with such a model while others are not [*Mitchell*, 1995] and more

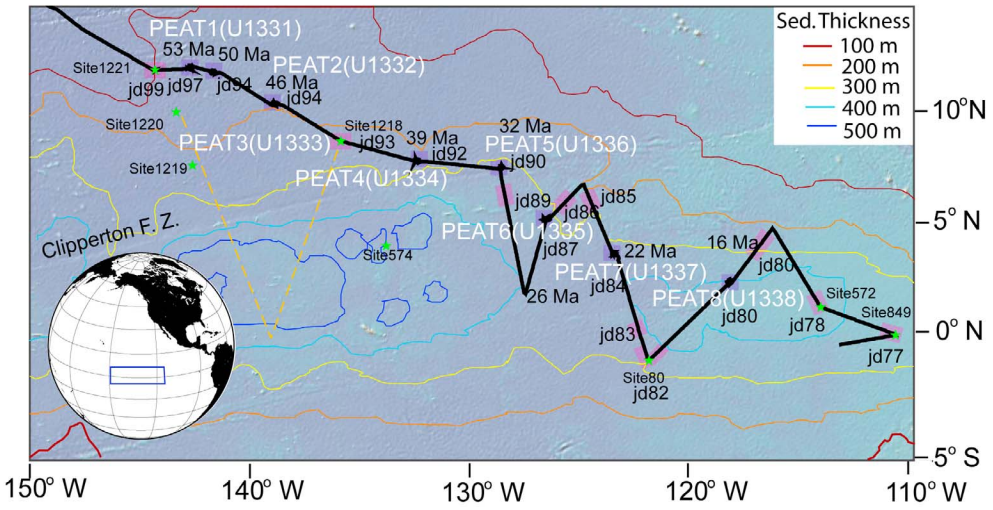

Figure 1. A map of AMAT03 seismic survey track line (solid black line) and locations of interpreted profiles in this study (pink and purple boxes; see details in text). The underlying bathymetry map is obtained from Global Multi-resolution Topography model (Marine Geoscience Data System [*Ryan et al.*, 2009]). Previously drilled sites are indicated with green stars. PEAT, Pacific Equatorial Age Transect. U1331–U1339 indicate sites drilled during IODP Expedition 320/321. Colored contour lines indicate the approximate sediment thickness based on *Mitchell et al.* [2003].

generally the question of whether sediment movements are consistent with the model is difficult to address because of a lack of in situ observations (these studies used either surface topography or subbottom profiles with penetration of ~50 m) [*Mitchell and Huthnance*, 2007]. Furthermore, we might not necessarily expect such models to apply in the Pacific given the more subdued topography of its abyssal hills.

[7] In this paper, we use digitally acquired seismic reflection records from an IODP site survey to study pelagic sedimentation in the equatorial Pacific, to reexamine pelagic sedimentation and to put constraints on the amount of focusing of sediments from abyssal hills to basins. We investigated the pelagic sedimentation regimes on 18–53 Ma ocean crust at the scale of abyssal hill topography by using both the new seismic interpretations from the AMAT-03 site survey and the results from Deep Sea Drilling Project (DSDP) and Ocean Drilling Program (ODP) drill sites in the equatorial Pacific. Our goals were to investigate (1) abyssal-hill-scale primary deposition regimes with respect to the equatorial high-productivity zone and (2) the extent to which seafloor topography has been subdued by preferential filling of abyssal valleys. At detailed study sites we used the seismic stratigraphy of *Mayer et al.* [1985, 1986] and *Bloomer et al.* [1995] to estimate ages of our interpreted seismic horizons ground truthed at seismic crossings of drill sites from DSDP and ODP.

2. Background

2.1. Eastern Equatorial Pacific Crust and Sediments

[8] The 0–53 Ma eastern equatorial Pacific seafloor has been formed at the fast spreading East Pacific Rise, with an average spreading half rate near the equator of ~70 mm/yr [*DeMets et al.*, 2010]. The seafloor moves to the northwest by Pacific plate motion [*Engebretson et al.*, 1984; *Sager and Pringle*, 1988; *Koppers et al.*, 2001; *Müller et al.*, 2008]. The depth of the seafloor ranges from ~2.8 km at the East Pacific Rise spreading axis and deepens to depths greater than 5 km for 50 Myr old crust because of cooling and thermal subsidence of lithosphere as it ages. The seafloor has low topography typical of fast spreading ridges, but still has a series of abyssal hills and basins [*Macdonald et al.*, 1996; *Menard and Mammerickx*, 1967], a few long-lived fracture zones [*Sandwell and Schubert*, 1982; *McCarthy et al.*, 1996], and many seamounts [*Jordan et al.*, 1983; *Smith and Jordan*, 1988] (Figure 1).

[9] For the most part, tropical Pacific sediments west of the East Pacific Rise are composed of the

remains of planktonic organisms. The thickness of sediment blanket in the eastern equatorial Pacific ranges from 100 to 800 m depending on the location and pathway of a given seafloor with respect to the equatorial high-productivity zone [*Mitchell*, 1998; *Moore et al.*, 2004; *van Andel and Moore*, 1974] The equatorial high-productivity zone is created by a narrow zone of divergence caused by the change in sign of the Coriolis effect at the equator elevating nutrients from the resulting upwelling. The maximum of sediment rain is at the equator, and the flux of particulate material decreases as the seafloor moves further north and away from this high-productivity zone [*Honjo et al.*, 1995]. The amount of sediments between distinctive seismic horizons thus thins away from the equator. Subsurface sediment layers can be correlated in sediment cores and seismic profiles over the thousands of square kilometers of the seafloor [e.g., *Lancelot and Larson*, 1975; *Mayer et al.*, 1985; *Shipboard Scientific Party*, 2002; *Lyle et al.*, 2010]. Drilling has shown that individual horizons are of the same age and indicates that equatorial Pacific pelagic sedimentation has >1000 km spatial scale, related to large-scale changes in the equatorial Pacific productivity regime. Outside the high-productivity zone, sediments deposited in this part of the Pacific are mostly composed of windblown brown clays and authigenic ferromanganese oxyhydoxides.

2.2. Information From Scientific Ocean Drilling

[10] DSDP Leg 85 [*Mayer et al.*, 1985] was the first drilling program in the equatorial Pacific using hydraulic piston coring technology, and the first to capture sediment sections with enough resolution to be compared in detail with digital seismic reflection data. ODP Legs 138 and 199 were designed as latitudinal transects across the paleoequator in order to study the changing patterns of sediment deposition across equatorial regions at critical time intervals of Earth's climate history. Leg 138 recovered late Miocene to recent intervals, while the Leg 199 drilling transect targeted the Paleocene/Eocene [*Pisias et al.*, 1995; *Lyle et al.*, 2002a].

[11] Major changes in carbonate burial have occurred over time because the carbonate compensation depth (CCD) has varied, sometimes rapidly. These carbonate variations are important to equatorial Pacific seismic stratigraphy because the physical property fluctuations (in particular changes in wet bulk density) caused by changes in carbonate content are key to making the acoustic reflection profile in the sediments [*Mayer et al.*, 1986]. Throughout the Eocene, the CCD was near a depth of 3.2–3.3 km, with some large short-term fluctuations [*Lyle et al.*, 2005; *Rea and Lyle*, 2005]. In the Neogene, the CCD was near 4.5 km, but also fluctuated, leaving distinctive sediment horizons [*van Andel and Moore*, 1974; *van Andel*, 1975; *Mayer et al.*, 1986; *Lyle*, 2003]. As will be discussed in sections 3.3 and 4.1, and most importantly for our study, site survey data for legs 85, 138, and 199 provided three significant studies on seismic stratigraphy in the equatorial Pacific. *Mayer et al.* [1985, 1986] identified the Neogene seismic horizons ("Green," "Magenta," "Purple," "Red," "Lavender," "Yellow," and "Orange"), while *Bloomer et al.* [1995] extended the stratigraphy into the eastern Pacific and added new horizons. *Lyle et al.* [2002b] identified the Paleogene seismic horizons P5, P4, P3, and P2. All of these seismic horizons correspond to strong changes in acoustic impedance, mostly through changes in carbonate content and associated changes in sediment wet bulk density, related to paleoceanographic events (see caption for Table 1).

[12] Recent Integrated Ocean Drilling Program (IODP) Expeditions 320 and 321 [*Pälike et al.*, 2008; *Lyle et al.*, 2010; *Pälike et al.*, 2010] together have reconstructed an essentially complete sediment column from the equatorial Pacific that links Leg 138 and Leg 199 drilling by an age transect ("flow line") backtracking the movement of the equatorial region on the Pacific plate [*Lyle et al.*, 2010]. The drilling and logging data from the expeditions sharpen our understanding of extreme changes of the CCD across major geological boundaries during the last 53 Myr. The drilling also provides ground truth for the seismic reflection profiles from the site surveys. The correspondence between AMAT-03 site survey names and the drilling are as follows: PEAT1 (Site U1331, 53 Ma crust), PEAT2 (Site U1332, 50 Ma crust), PEAT3 (Site U1333, 46 Ma crust), PEAT4 (Site U1334, 39 Ma crust), PEAT5 (Site U1336, 32 Ma crust), PEAT6 (Site U1335, 26 Ma crust), PEAT7 (Site U1337, 24 Ma crust), and PEAT8 (Site U1338, 18 Ma crust) (Figure 1). Because the Pacific plate has moved WNW throughout this time interval, each site crosses the equatorial high-productivity zone at progressively younger ages. Only younger age sites (U1337 and U1338) recovered sedimentary sections of the late Miocene-Holocene with relatively high sedimentation rates and preserved carbonate (both with rates ~15 m/Myr [*Lyle et al.*, 2010]). Drill sites on older crust (U1331–U1336) experienced low sedi-

Table 1. First-Order (Best Estimates to Date) Seismic Interpretation: PEAT Sites[a]

Horizon	TWT	Age
PEAT1C Line 8 (Time 0557 UT)		
SF	0	0
P3	94.5	33
P2	192.5	48
BM	239	53
PEAT 2C Line 6 (Time 1752 UT)		
SF	0	0
P3	137	33
P2	161.5	48
BM	212	50
PEAT3C Line 3 (Time 2027 UT)		
SF	0	0
P4	0	30
P3	77	33
P2	133	43
BM	222.5	46
PEAT 4C Line 1 (Time 0219 UT)		
SF	0	0
Orange (O)	22	24.6
P5	171	27
P4	213	30
BM	337.5	39
PEAT 5C Line 6 (Time 1108 UT)		
SF	0	0
Purple	39	10
Red	101	15
Lavender	151	17
Yellow	184.5	23
Orange (O)	214.5	24.6
P5	264.5	27
BM	324.5	32
PEAT 6C Line 8 (Time 0815 UT)		
SF	0	0
Purple	153.5	10
Lavender	301	17
BM	441.5	27
PEAT 7C Line 4 (Time 1654 UT)		
SF	0	0
Purple	68	10
Lavender	253	17
BM	532	24
PEAT 8C Line 1 (Time 1742 UT)		
SF	0	0
Purple	318	10
BM		

[a]Seismic event ages are from *Mayer et al.* [1985, 1986], *Bloomer et al.* [1995], and *Lyle et al.* [2002b], and site locations, interpreted horizons, and ages of the interpreted horizons are based on ESPS_summary_IODP_Proposal626. SF, seafloor; Purple, 9.6–10.5 (Ma); Red, 13.5–15.0 (Ma); Lavender, 15.7–17.0 (Ma); Yellow, 19–23 (Ma); Orange (O), 21.5–24.6 (Ma); P5 = 27 (Ma); P4 = 30 (Ma); P3 = 33 (Ma); P2 = 43–48.4 (Ma); BM, basement; TWT (msbs), two-way travel time in milliseconds beneath seafloor (msbs).

mentations rates or hiatuses. In contrast, sediments of Eocene age are only found at the sites on older crust with Paleogene equator crossings, e.g., Sites U1331–1334. More detailed summaries of lithology, physical properties, and biostratigraphy are given by *Pälike et al.* [2010].

2.3. Pelagic Sedimentation Regimes

[13] The sedimentation regime of the deep seafloor can be affected by many physical factors, such as internal waves [*Lister*, 1976; *St. Laurent and Garrett*, 2002], quiescent currents over topographic depressions [e.g., *Flood*, 1988; *Mitchell and Huthnance*, 2007], deep-sea flows [*Lonsdale and Smith*, 1980; *Sen et al.*, 2008; *Arbic et al.*, 2009], bioturbation [*Meadows and Meadows*, 1994], lateral and vertical sediment transportation by erosion [*Culling*, 1962; *McCave*, 1984], erosion by accelerating tidal currents around topography forming moats around topographic highs [*Roberts et al.*, 1974; *Heezen and Rawson*, 1977], dissolution due to hydrothermal venting [*Bekins et al.*, 2007; *Moore et al.*, 2007], and dissolution of carbonate by subsidence of the seafloor and by changes in ocean-atmosphere interactions [*Lyle*, 2003]. It is important when characterizing basin-scale sedimentation regimes to understand how sediments accumulate over time at abyssal seafloor. However, because of the interacting processes, it has been challenging to both observe and model the physics of pelagic sediment regimes.

3. Methods

3.1. Data Collection

[14] Seismic horizons were interpreted from a multichannel seismic reflection and data collected during the AMAT03 cruise (March–April 2004) on R/V *Revelle* (note that data are archived at the Marine Geoscience Data System UTIG portal (http://www.ig.utexas.edu/sdc/, cruise AMAT03RR)). For the entire survey period, seafloor bathymetry was acquired by high-resolution shallow penetration Simrad EM120 shipboard multibeam echosounder and the along-track subbottom information was obtained by Knudsen 320B dual-frequency chirp sonar, the data from which were also archived in the Marine Geoscience Data System at UTIG. The multibeam data were manually cleaned of artifacts (ping-edited) and gridded with MBSystem software (available at http://www.ldeo.columbia.edu/res/pi/MB-System/). The raw multibeam data are archived at the Scripps Geologic Data Center (http://gdc.ucsd.edu/index.php?page=0).

Table 2. Parameters for Seismic Processing

	Streamer Type	
	4 Channel	48 Channel
Sampling interval	0.5 ms	0.5 ms
Group (receiver) interval	50 m	12.5 m
Source (shot) interval	31 m	24.7 m
CDP bin	25 m	6.25 m
Water velocity	1480 m/s	1480 m/s

[15] Seismic reflection data were acquired along a total of ~6145 km of survey line that followed an equatorial age transect (Figure 1). This survey crossed 10–53 Ma seafloor and extends over the area between 150°W–110°W and 5°S–15°N. The seismic survey lines also cross the following drill sites for ground truth (Figure 1): ODP Site 849, DSDP 572, and 80, and IODP Sites U1331–1338. We used a 4-channel Sercel streamer at ~10 knots during underway surveys and a 48-channel Geometrics GeoEel streamer at ~6 knots at most of the PEAT site surveys. The seismic source was two 150 c.i. generator/injector (GI) guns fired at 10 s intervals for both 4- and 48-channel operations. Data were recorded with a 0.5 ms sampling interval and 8 s record length. No analog high- or low-cut filter was applied during recording.

[16] We chose a total of 8 survey segments at PEAT drill sites, and 10 segments of the underway seismic reflection profiles to study (Figure 1). For underway profiles, we selected continuous 70–180 km (4 to 8 h at 10 knots) seismic profile segments from various latitudes and with variable crossing angles with respect to the strike of abyssal hills to cover a variety of pelagic sedimentation environments (pink boxes, julian day (jd) 77, jd78, jd80, jd82, jd83, jd85, jd86, jd89, jd93, and jd99 in Figure 1). Five of these segments cross drill sites, ODP Site 849, 572, 1218, and 1221, and DSDP Site 80 to correlate our seismic interpretations with previous site survey results and results from these drilled holes. Within the PEAT survey sites, we selected profiles that are nearly perpendicular to the strike of abyssal hills [e.g., *Kriner et al.*, 2006] to obtain the data coverage over topographic highs and lows (purple boxes, P1–P8 in Figure 1; Site bathymetry and track lines are available from *Pälike et al.* [2010]).

3.2. Multichannel Seismic Reflection Data Processing

[17] Acquired multichannel seismic reflection data were processed using Landmark ProMax™ software. The processing flow consisted of band-pass filtering, geometry assignment, CDP ensemble stacking with normal move out, and F-K migration assuming 1480 m/s constant P wave velocity (Table 2). For trace display and subsequent interpretation, we often used both high- and low-cut band-pass filter (e.g., 25–50–300–600 Hz) to minimize noise and sharpen changes in the polarity of seismic wave at seafloor and subsurfaces.

3.3. Seismic Interpretation

[18] For the selected seismic profile segments in this study, we interpreted seismic horizons in each selected profiles based on previous interpretations [*Mayer et al.*, 1985, 1986; *Bloomer et al.*, 1995; *Lyle et al.*, 2002b], then additionally interpreted horizons with distinctive changes in reflection amplitudes (Text S1).[1]

[19] In order to ground truth the seismic reflection data, we first examined the correlative paloceanographic events between Sites 574 and 849 seismic reflectors [*Bloomer et al.*, 1995]. Sites 574 and 572 are located nearly 500 and 2000 km to the west of Site 849, respectively (Figure 1). We next correlated downhole data obtained in Ocean Drilling Project (ODP) Sites 574 [*Mayer et al.*, 1985, 1986], 572, and 849 [*Bloomer et al.*, 1995] check the sites and references one more time (Figure 2a). In this exercise, we found that the comparison of downhole carbonate content (%) profiles for Site 849 and 572 and of downhole porosity (%), density, and velocity profiles for Site 572 and 574 are particularly useful (Figure 2b). The resulting correlations become tie points from one site to the other in our study.

[20] There is a 20 ms offset at the basement reflector in between seismic data given by *Bloomer et al.* [1995] and AMAT03 seismic profile jd77, each survey line of which has different trajectory with respect to the location of Hole 849B. This offset can be explained by differences in seismic source (e.g., water gun versus air gun) and the geometry of the streamers. We compared *Bloomer et al.*'s [1995] traveltime and depth relationship to the velocity data acquired by sonic log in Hole 849B during ODP Leg 138 to see how close the interpreted horizons in this study are to Bloomer's seismic stratigraphy. The comparison confirms that depths of our interpreted seismic horizons derived from Hole 849B logging are very close to that of

[1] Auxiliary material data sets are available at ftp://ftp.agu.org/apend/gc/2010gc003347. Other auxiliary material files are in the HTML.

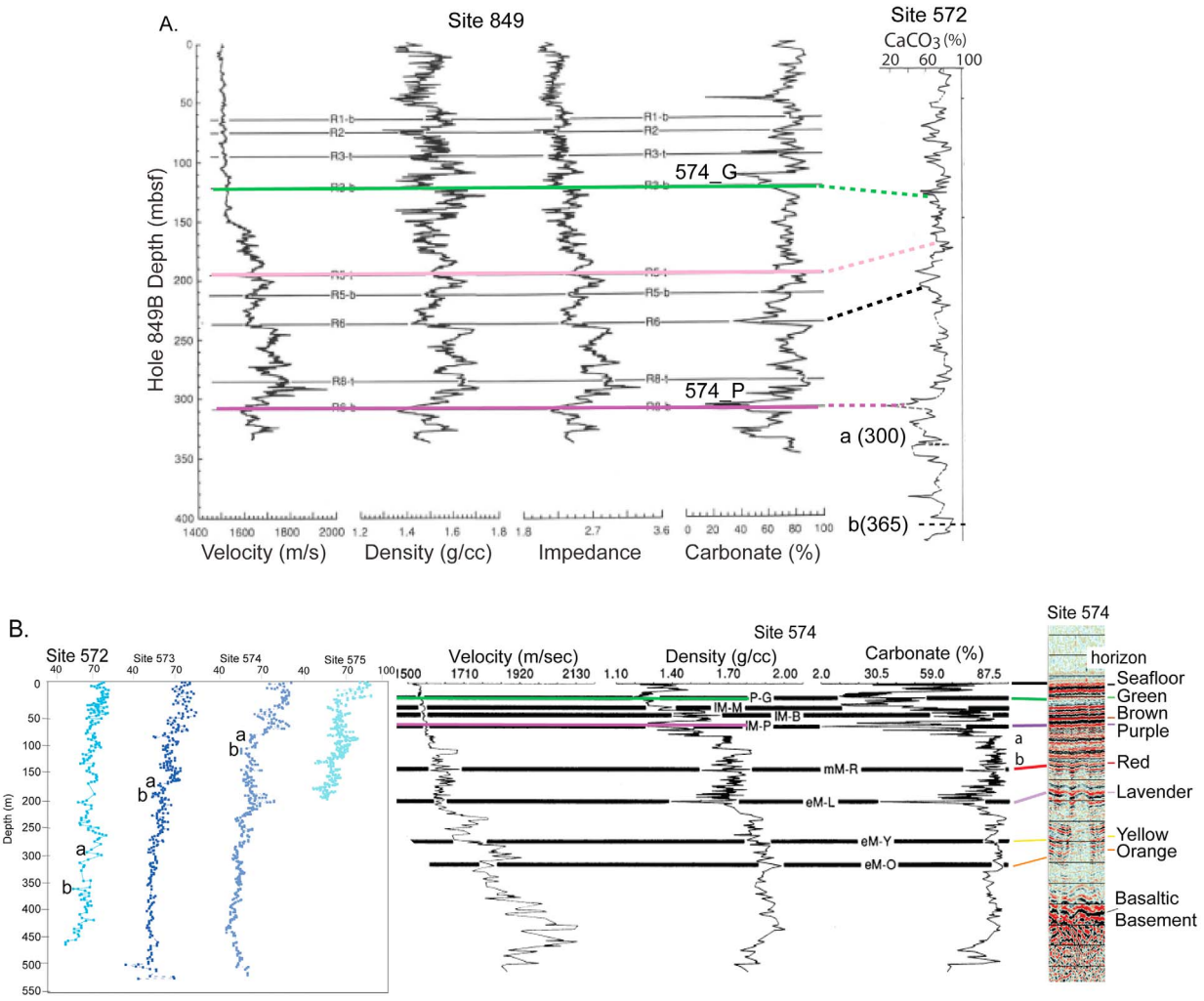

Figure 2. (a) The cross-hole correlations between downhole logging results. Logging data correlation between Site 849 [*Bloomer et al.*, 1995] and Site 572. (b) Physical properties data correlation between Sites 572 [*Wilkens and Handyside*, 1985] and 574 [*Mayer et al.*, 1986] (reprinted with permission from AAAS) with seismic interpretation near Site 574.

Bloomer et al.'s [1995] seismic interpretation with negligible offset (Table 3). This exercise suggests that *Bloomer et al.*'s [1995] seismic stratigraphy can readily become a template in this study.

[21] For sites jd77–jd89 that are located the south of the Clipperton Fracture Zone, we correlated interpreted horizons in each of our selected sites with previously determined seismic horizons by locating Green, Magenta, and Purple horizons [*Mayer et al.*, 1985; *Bloomer et al.*, 1995]. For sites jd80 jd99 that are located north of the Clipperton Fracture Zone (Figure 1), we correlated seismic horizons from *Lyle et al.* [2002b] with interpreted seismic horizons in each of our study sites (Figure 2).

[22] After locating all the correlatable horizons at each of selected study sites, we assigned the ages of the horizons based on the biostratigraphy from Leg 199 [*Barron et al.*, 2004; *Nigrini et al.*, 2006] and seismic stratigraphy by *Lyle et al.* [2002b] (Figure 3). We then approximated the timing of the equator crossing at each site to locate the interval with the possible maximum sedimentation rate at each study site. We calculated paleocolatitude of a given site of the Pacific plate based on the relationship between the Pacific plate motion and the rotation of the Euler poles [e.g., *Engebretson et al.*, 1984; *Gripp and Gordon*, 1990]. We approximated latitudinal plate motion as 0.25°/Myr northward. Based on these calculations, assigned

Table 3. Comparison Between Site 849 Seismic Stratigraphy by *Bloomer et al.* [1995] and Site 849 Sonic Log From This Study[a]

Horizons	TWT1 (msbs)	Depth1 (m)	TWT2 (msbs)	DTLF2 (m)	DTLN2 (m)
R1-b	85	64.8	85	63.0	63.8
R2	100	76.2	100	74.4	74.9
R3-t	118	89.3	125	93.4	93.9
R3-b (G)	161	122.6	160	120.5	120.8
R5-t (M)	255	196.7	260	200.7	200.7
R5-b	275	213.4	280	217.2	217.3
R6	307	239.6	310	242.3	242.4
R8-t	354	280.5	340	267.7	267.9
R8-b (P)	376	299.9	385	306.5	307.0

[a]Horizons are interpreted seismic horizons by *Bloomer et al.* [1995]. TWT1 and Depth1 are two-way travel time in miliseconds beneath the seafloor and suggested depths from *Bloomer et al.* [1995]. TWT2, DTLF2, and DTLN2 are two-way travel time in milliseconds beneath the seafloor interpreted in this study and depth detected by far- and near-receiver on sonic log tool strings. Depth conversions for DTLF2 and DTLN2 are based on best fit curves ($R \approx 1$) to the log data: DTLF2 (depth) = $0.609 + 0.717x + 0.0002x^2$, and DTLN2 (depth) = $2.2114 + 0.705x + 0.000223x^2$, where x is TWT2.

ages of the interpreted seismic horizons, and the approximate basement age of each study site, we identified the likely timing of equator crossing (Figure 3).

3.4. Sedimentation in Relation to Abyssal Hill Topography

[23] We evaluated horizontal transport on the 10–100 km scale and preferential basin filling processes by observing the relative rates of sedimentation over abyssal hills and basins over time. As a measure of the degree of basin filling, we calculated changes in curvature at the minima of the fitted curves by fitting a 2-D polynomial curve (parabola) (Figure 4). Whereas previous studies of Atlantic basin infilling have sought to determine if sediment surfaces have simple parabolic shapes, which are steady state solutions to the diffusion transport model equation [*Mitchell*, 1998; *Webb and Jordan*, 2001a], our first-order observation on the interpreted seismic horizons suggests that the Pacific basins we studied have more complicated sedimentation histories than the Atlantic Ocean basins, and we observe changes in basin filling style both laterally and vertically. The choice of a 2-D polynomial curve to represent infilling is based on *Mitchell* [1995, 1998].

4. Results

4.1. Distribution of the Prominent Seismic Horizons in the Equatorial Pacific

[24] We made our seismic interpretation by making "reflector packets," the top and bottom of which are marked by distinctive impedance changes resulted in not only identifying previously identified seismic horizons but also picking other unnamed horizons (Text S1). We used three prominent features in our seismic profiles for our interpretation: the basement reflector, the purple horizon of *Mayer et al.* [1985], and the topmost transparent layer (above the orange horizon) that extends across a wide geographical region north of about 7°N. The purple horizon [*Mitchell et al.*, 2003] is associated with an extreme carbonate minimum in the sediment column, where the lithology change generates a strong impedance contrast [*Mayer et al.*, 1985]. The topmost transparent layer is likely to be a red clay layer with extremely slow accumulation rates after a site passed below the CCD [*Bryant and Bennet*, 1988; *Lyle et al.*, 2002a]. This top seismic horizon is time transgressive, since it depends on both the ocean carbon cycle and the local seafloor depth.

[25] Using these three prominent reflectors as distinctive markers, we interpreted sediment packets between the sites located at south and north of PEAT5. The Purple horizon can be correlated over >20° in longitude (>2160 km) and ~8° in latitude on Pacific plate crust formed after 33.6 Ma (Eocene-Oligocene boundary; from Site 849 to Site 574, to PEAT6 (Site U1335) in Figure 3). Site 849 is on the youngest crust capable to have this horizon. The event can be tracked 10° westward of Site 574 [*Mitchell et al.*, 2003], but drill sites are lacking to confirm the interpretation. Above the purple horizon, the sediment packet contains a series of large changes in impedance. Below the purple horizon, the sediment has only small amplitude seismic reflections, indicating that changes in impedance and lithology are smaller.

[26] In our data, the transparent sediment package, defined by the purple reflector and below, disappears west of jd90PEAT5 (~32 Ma) and north of the Clipperton Fracture zone, because of slow

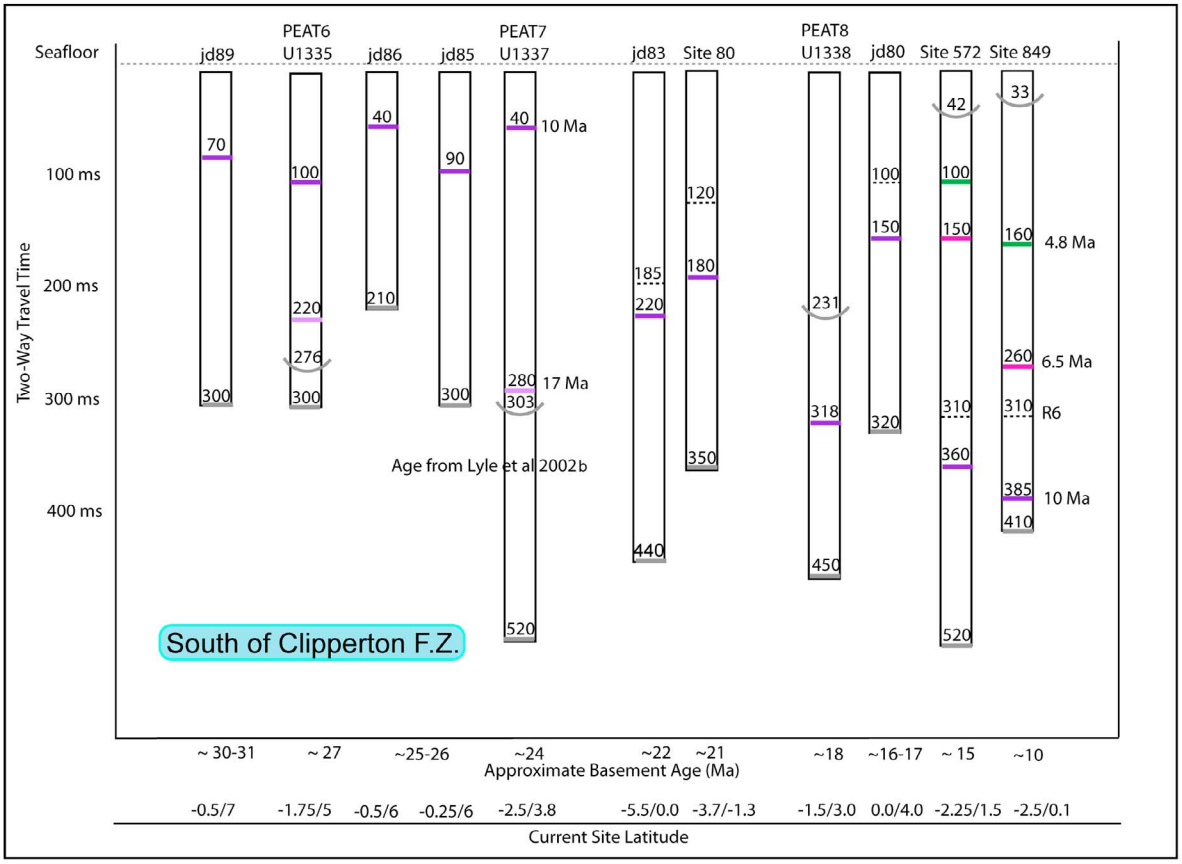
Seafloor
Two-Way Travel Time
100 ms
200 ms
300 ms
400 ms
jd89
PEAT6 U1335
jd86
jd85
PEAT7 U1337
jd83
Site 80
PEAT8 U1338
jd80
Site 572
Site 849
70
300
100
220
276
300
40
210
90
300
40
10 Ma
280
303
17 Ma
520
185
220
440
120
180
350
231
318
450
100
150
320
42
100
150
310
360
520
33
160
4.8 Ma
260
6.5 Ma
310
R6
385
10 Ma
410
Age from Lyle et al 2002b
South of Clipperton F.Z.
~ 30-31
~ 27
~25-26
~24
~22
~21
~18
~16-17
~ 15
~10
Approximate Basement Age (Ma)
-0.5/7
-1.75/5
-0.5/6
-0.25/6
-2.5/3.8
-5.5/0.0
-3.7/-1.3
-1.5/3.0
0.0/4.0
-2.25/1.5
-2.5/0.1
Current Site Latitude

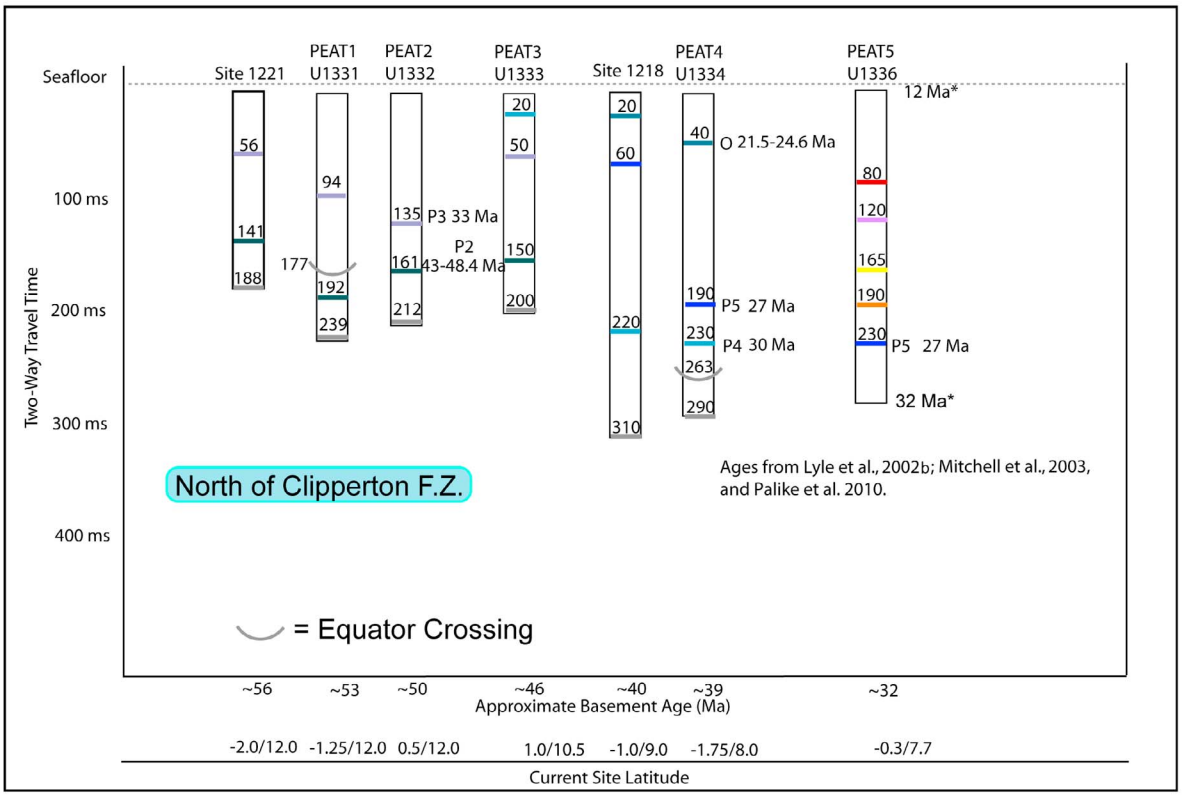
Seafloor
Two-Way Travel Time
100 ms
200 ms
300 ms
400 ms
Site 1221
PEAT1 U1331
PEAT2 U1332
PEAT3 U1333
Site 1218
PEAT4 U1334
PEAT5 U1336
56
141
188
94
177
192
239
135
P3 33 Ma
P2
161
43-48.4 Ma
212
20
50
150
200
20
60
220
310
40
O 21.5-24.6 Ma
190
P5 27 Ma
230
P4 30 Ma
263
290
12 Ma*
80
120
165
190
230
P5 27 Ma
32 Ma*
North of Clipperton F.Z.
Ages from Lyle et al., 2002b; Mitchell et al., 2003, and Palike et al. 2010.
= Equator Crossing
~56
~53
~50
~46
~40
~39
~32
Approximate Basement Age (Ma)
-2.0/12.0
-1.25/12.0
0.5/12.0
1.0/10.5
-1.0/9.0
-1.75/8.0
-0.3/7.7
Current Site Latitude

Figure 3

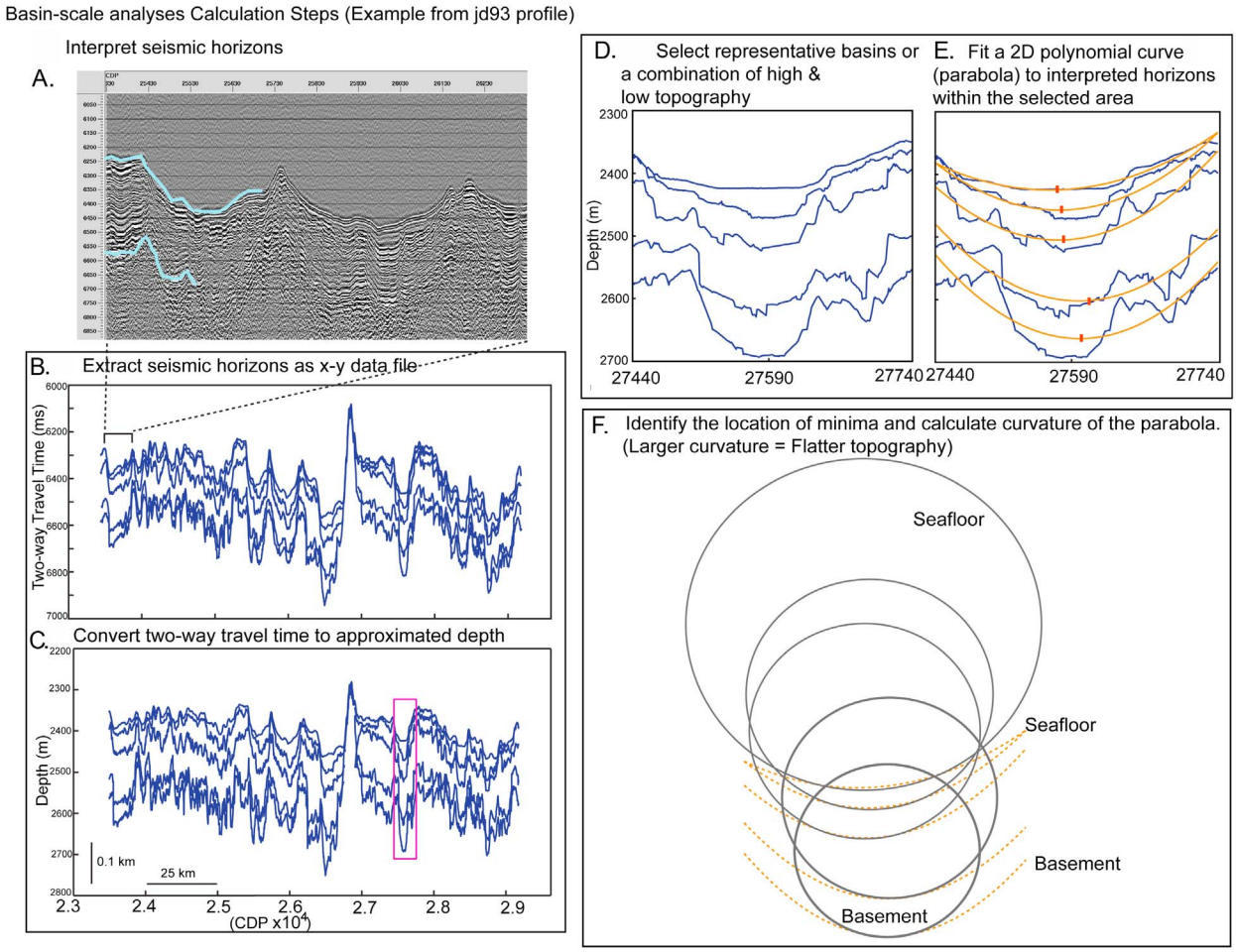

Figure 4. The summary of calculation steps for the basin filling analyses. We selected representative basins or regions with a combination of high and low topography from each study site and fit a best fit 2-D polynomial curve for each interpreted horizon. Fitting the 2-D polynomial curve can serve two purposes in basin-scale analyses: to quantify flattening in topography and to evaluate a diffusion/erosion basin filling model. A simple model of a basin filling with a constant flux implies that a parabola is appropriate [e.g., *Mitchell*, 1995].

sedimentation and high levels of dissolution as the seafloor deepens. The topmost transparent layer overlies a thick, low-amplitude packet, the base of which is marked by orange horizon. The transparent layer becomes prominent from jd90PEAT5C to jd93PEAT3C. From past ODP drilling, this transparent layer is identified as pelagic clay and is identified in all the sites located at the north of the Clipperton Fracture zone (jd9) except for jd99Site 1221 [*Pälike et al.*, 2009].

4.2. Seismically Identified Carbon Compensation Depth

[27] A surface transparent layer can first be found a few tens of kilometers northwest from the beginning of jd91 about 200 km north of the Clipperton fracture zone (~6.5°N, 126.5°W, and to the west); Figures 1 and 5). The age of the seafloor is slightly older than 32 Ma and this part of the seafloor has

Figure 3. The summary of seismic horizons observed from each study profile in milliseconds two-way travel time (TWTT). The sites (and site names) correspond to those shown in Figure 1. We selected horizons in the undisturbed sediments over moderate topography for non-PEAT sites and the exact locations of drilled sites for PEAT sites. The correlated horizons are color coded following *Mayer et al.* [1985, 1986] and *Lyle et al.* [2002b]. Approximate crustal ages and current site latitudes are also shown (see section 3). Dates with asterisks are determined biostratigraphy during IODP Expedition 320/321 [*Pälike et al.*, 2010].

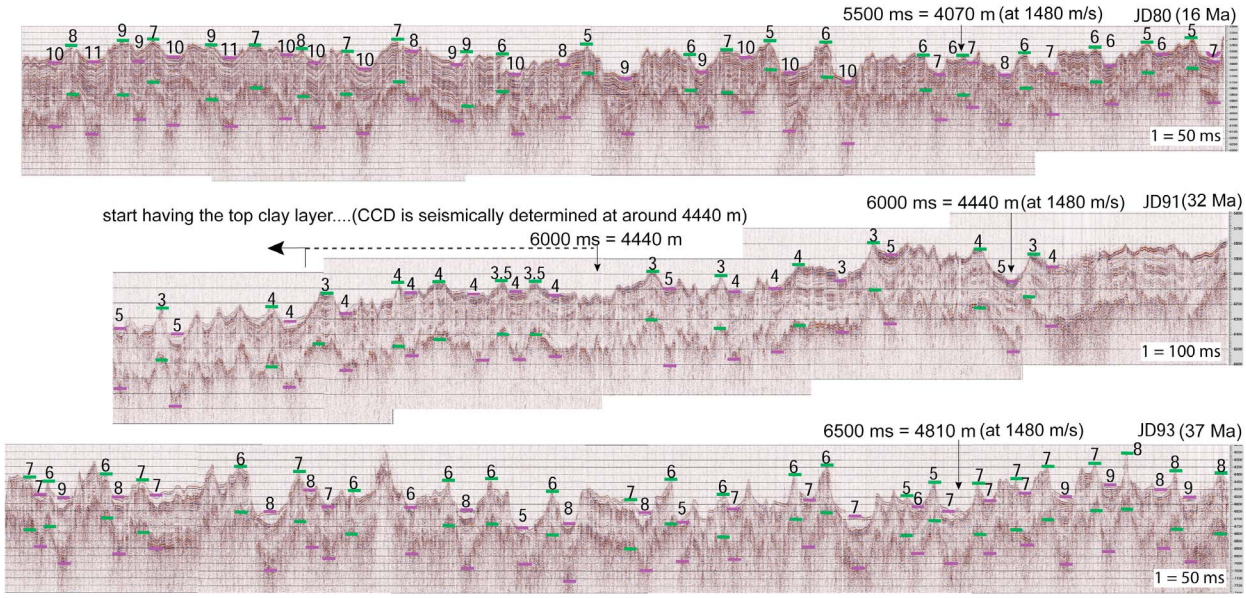

Figure 5. A part of three representative sedimentation regimes from 24 h underway seismic profiles of jd80 (16–18 Ma crust), jd91 (32–37 Ma), and jd93 (37–43 Ma). All of the profiles are after migration. Green and purple bars show the thickness of sediments in topography high and low, respectively, with a unique scale in each profile for better magnification (1 = 50 ms in jd80, 100 ms in jd91, and 50 ms in jd93). The data for the complete 24 h seismic profiles are available in Table 4.

extremely low sedimentation rates, where biogenic sediments mostly dissolve before burial (see section 4.4). We propose that the depth where the topmost transparent layer can be seismically identified to be the location of the CCD. A distinct transparent layer appears at a two-way travel time (TWTT) of 6000 ms or 4440 m water depth using 1480 m/s for the TWTT for the water column. For comparison, *Farrell and Prell* [1989] identified the Pleistocene CCD south of the Clipperton Fracture Zone to be about 4800 m, and *Berger et al.* [1976] found the CCD to be between 4400 and 4800 m in the general vicinity of the AMAT03 track. We expect the CCD to the south of the Clipperton Fracture Zone to be deeper than to the north because the net flux of $CaCO_3$ rain is greater and greater levels of dissolution are needed to remove the additional $CaCO_3$.

4.3. Basement and Seafloor Topography

[28] Basement topography over the study sites is characterized by abyssal hills and basins, typical of fast spreading normally faulted crustal topography [e.g., *Buck et al.*, 2005]. This part of the Pacific seafloor was formed at the mid-ocean ridge system without late stage local tectonic reconfigurations. Abyssal hills in our study area are formed at fast spreading East Pacific Rise and the typical height of the hills measured from the seismic profile is ~400 m (see the profiles perpendicular to the abyssal hill strikes in Figures 5 and S1) and the distance from a top of the hill to the next (the width of abyssal basins) is ~10 km. These length scales are consistent with other observations and the proposed formation process for abyssal hills on fast spreading crust by, e.g., *Goff* [1991] and *Macdonald et al.* [1996]. As will be discussed in section 5, this basement topography is somewhat subdued by sediment burial and the amount of smoothing depends on the thickness of overlying sediment blanket. Nevertheless, the sediment-covered seafloor still retains the signature of the basement abyssal hills throughout the entire study area (see jd80 versus jd93 in Figure 6).

[29] Several different faults and associated sedimentation anomalies are observed in our study sites. Although these are minor features in the basement structure compared to the crustal-scale abyssal hills and basins initiated by along-axis normal faults at mid-ocean ridges (Figure 7) [*Small*, 1994; *Macdonald et al.*, 1996], these subsurface features result from local dynamics that may affect local sediment redistribution and trigger sediment movement or expose a sediment surface to dissolution as a consequence. These features, in terms of the timing of fault formations and asso-

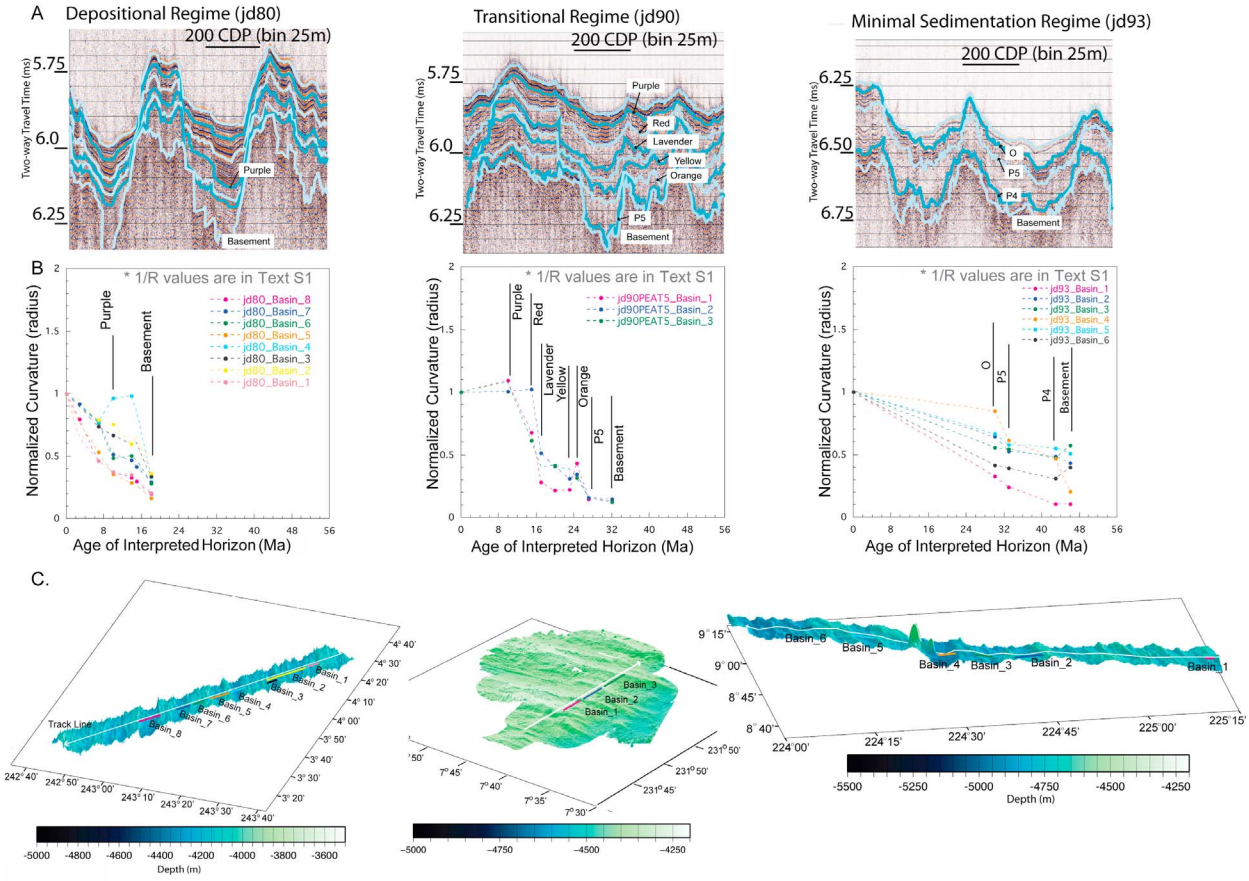

Figure 6. Examples of abyssal hill basin filling processes from representative profiles within the depositional (jd80), transitional (jd90), and minimal sedimentation regimes (jd93). (a) Seismic profiles, (b) the growth of curvature from the basement to the seafloor (see the text for detailed calculations), and (c) multibeam bathymetry profiles. Additionally, the radii of the curvature of each profile and other basin data are available in Text S1.

ciating sediment reworks, can be categorized into three types:

[30] 1. One type consists of recently formed faults. The timing of their formation is manifested by the vertical extent of the faults cutting through the entire sediment packet. They make a sharp contact at the sediment/water interface (Figure 7b).

[31] 2. Another type includes multiple generations of faults in the same locale: An older fault and dislocation appear to be covered by sediments and followed by a new fault cutting entirely through the surface sediment layer (Figure 7c).

[32] 3. A few different kinds of paleofaults are completely buried by sediments.

[33] Where basement topography is buried underneath a significant accumulation of new sediments (Figure 7d), seafloor topography near the fault is not only affected by the faulting but also by processes that affect the sediment blanket (Figure 7e). Basement topography is still retained but erosion can often be observed in the vicinity (Figure 7f). The origin of the late stage faults is not known and might result from multiple causes. They may be caused by extended deforming plate boundary (far-field stress field) as was observed by *Wilcock et al.* [1992] and *Lee and Solomon* [1995], or they may be associated with cracking lithosphere [e.g., *Sandwell and Fialko*, 2004; *Korenaga*, 2007]. The three different types of faults probably help to form fluid pathways in intraplate settings [e.g., *Moore et al.*, 2007; *Bekins et al.*, 2007].

4.4. Sedimentation Regimes

4.4.1. Large-Scale Sedimentation Regimes in the Eastern Equatorial Pacific

[34] In the eastern Pacific, the overall thickness of the entire sediment blanket, estimated with 1480 m/s constant velocity, ranges from >400 ms (>320 m

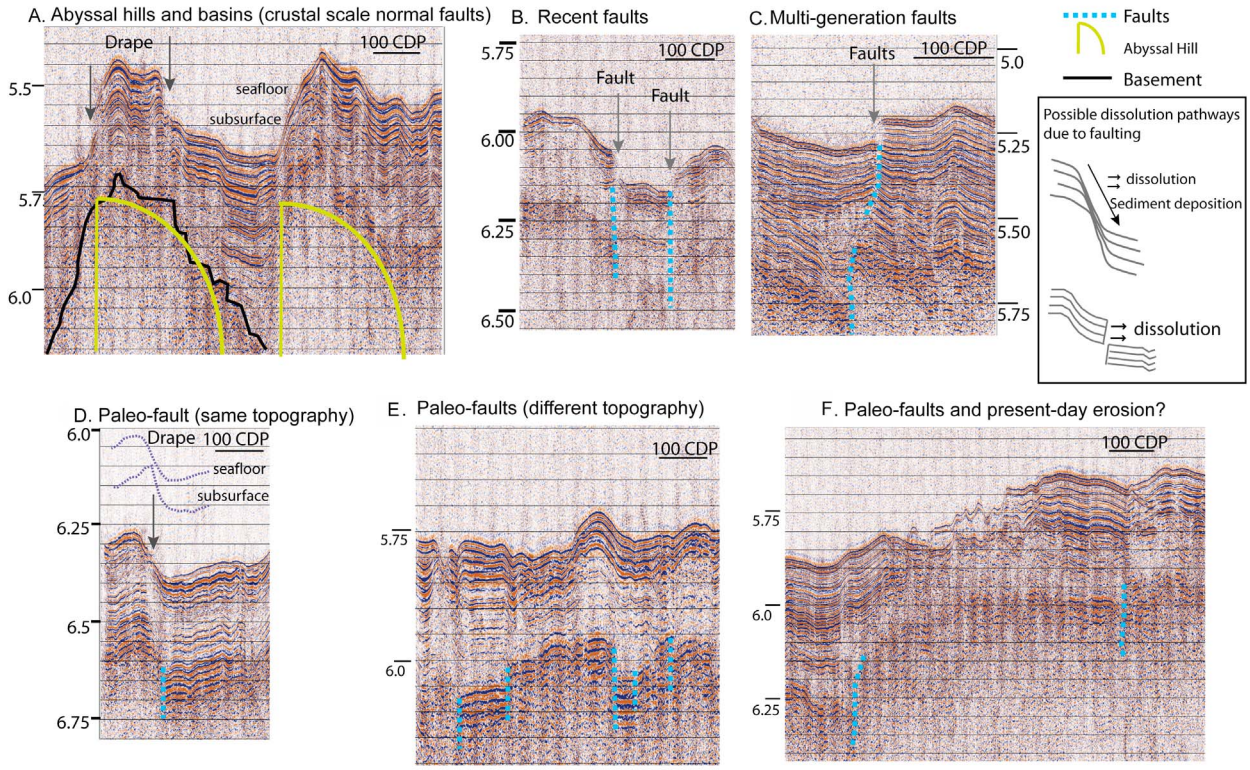

Figure 7. Four types of faulting observed in our study sites (see detailed interpretations in section 4.3).

sediment cover) to slightly less than 100 ms (~80 m), thinning from east to west and to the north away from the equator (Figure 3). The thickness of sediments we observed conforms with the geographic dimensions of the equatorial sediment mound [*Mitchell*, 1998; *Mitchell et al.*, 2003].

[35] The sediment blanket observed in AMAT03 survey has three overall sedimentation regimes: sediments deposited with relatively high sedimentation rates (*depositional* regime, average sedimentation rates ≥20 m/Myr) low sedimentation rate regimes (*minimal sedimentation*, average sedimentation rate <5 m/Myr), and a *transitional* regime between the end-members. These regimes are defined by location with respect to the equatorial high-productivity zone. The 18 study sites studied in this paper are roughly categorized as follows:

[36] 1. Depositional regimes (Site 849, Site 572, PEAT8 (U1338), PEAT7 (U1337)) have thick carbonate sediment cover due to the crust being within the equatorial high-productivity zone from near the age of crustal formation through the Holocene.

[37] 2. Under transitional regimes (j80, Site80, jd83, jd85, jd86, PEAT6(U1335), jd89, PEAT5 (U1336)), distinctive equatorial zone carbonate sediments were deposited significantly before the Holocene followed by a period when the sediment column has been moved away from under the equatorial productivity zone.

[38] 3. Minimal sedimentation regimes (PEAT4, Site1218, PEAT3, PEAT2, PEAT1, Site 1221) include dissolution of carbonates and biogenic silica before burial and deposition of noncarbonate (clay and siliceous) sediments. The top clay layer seems to respond differently to the movement of the ambient water than the underlying biogenic carbonate deposits, often resulting in asymmetric distribution of sediments deposited in basins north of the Clipperton Fracture Zone.

4.4.2. Abyssal-Hill-Scale Sedimentation

[39] The sediment regimes affect how sediment has been redistributed between abyssal hills and abyssal basins. Overall, we observed that depositional and transitional regimes have symmetric drape of sedimentation within basins and subdued topogra-

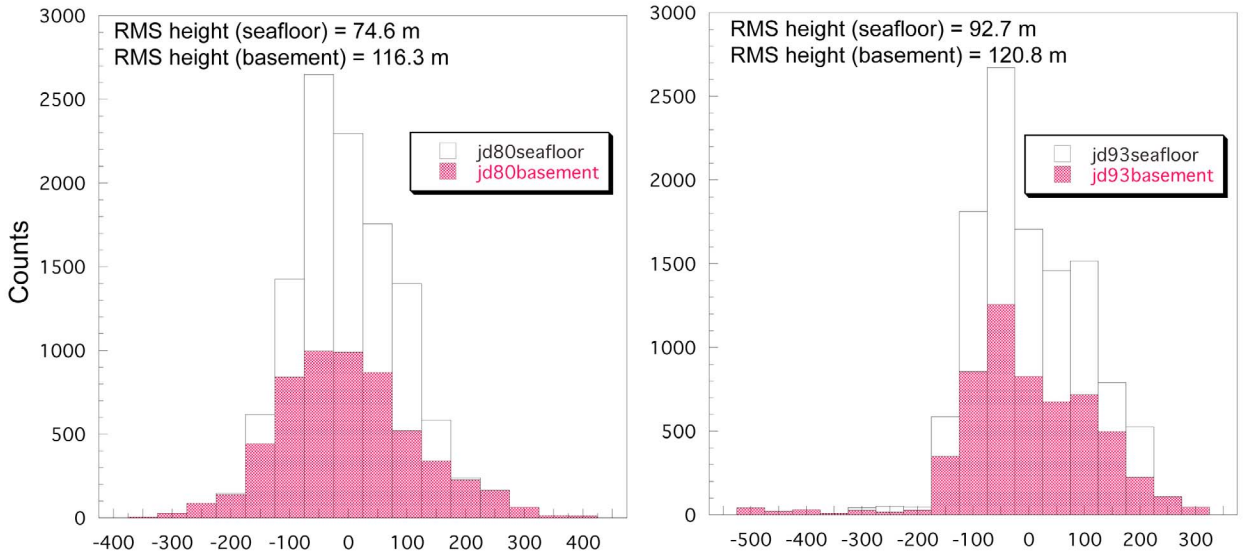

Figure 8. Histograms showing the roughness of the seafloor and basement topography of depositional (jd80) and minimal sedimentation (jd93) regimes.

phy, whereas minimal sedimentation regimes have more drape of sedimentation within topographic lows and higher seafloor relief.

[40] Using the change in radius of parabolas fitted to seismic horizons from the basement to the seafloor, we can evaluate different stages of basin filling. We normalized the curvature from each basin in each selected area to compare changes in flattening among basins in the selected areas, in essence assuming fractal scaling (Figure 4). An increase in the radius of the parabola indicates a flattening of the seafloor topography and preferential infilling of the basin.

[41] Representative profiles from the sedimentation regimes show how the basins were filled over time (Figure 6 and Text S1). Both in the depositional and minimal sedimentation regimes, sediments fill the basins almost linearly with age. On the other hand, it is clearly shown that in the transitional regime, the basins were preferentially filled when the seafloor experienced the highest sedimentation rates, i.e., when the seafloor crosses the equatorial high-productivity zone (Figure 1) [*Mitchell et al.*, 2003]. This observation supports the idea that these three sedimentation regimes host distinct basin-filling processes.

4.5. Topography Reduction and Its Implications

[42] We also examined sedimentation processes in a wider geological context. We chose three longer profiles to specifically examine (1) how the seafloor topography has been changed over time in different sedimentation regimes and (2) to what extent the seafloor topography has been subdued by basin flattening ("sediment focusing") in different sedimentation regimes. Each profile represents approximately 500 km length (24 h at 10 knots) of the seafloor in the depositional regime (jd80), transitional regime (jd91), and minimal sedimentation regime (jd93) (Figure 5; see also the high-resolution, large size version in Figure S1).

[43] We investigated the evolution of seafloor topography over time in different sedimentation regimes by calculating root-mean-square (RMS) height of topography of both seafloor and the basement [*Goff and Jordan*, 1988, 1990; *Webb and Jordan*, 1993] as well as making histograms of the deviations in the seismic depths from the mean values along profiles from the two end-member sedimentation regimes. This simple statistic shows the roughness of the basement and seafloor topography in each sedimentation regime.

[44] In both depositional and minimal sedimentation regimes, the distributions of the deviations of basement and seafloor are almost the same, except the distribution of basement topography has wider "tails," i.e., the basement is rougher than the sediment covered seafloor, and sediment is being preferentially deposited in basins, thus smoothing relief (Figure 8). The RMS heights of the seafloor indicate that seafloor topography in the equatorial Pacific is not completely smoothed out even after

tens of millions of years regardless of the sedimentation rates and regimes.

[45] Within the depositional regime, where the basaltic basement topography completely buried by hundreds of meters of sediment, much of the basement relief remains at the seafloor despite deep burial (e.g., RMS seafloor height for depositional regime is 74.6 m). It is characteristic of the depositional regime that the topography is being subdued over time, with a relatively steep slope to change in curvature versus age (Figure 6).

[46] In contrast, in the minimal sedimentation regime, whether the topography has been smoothed out depends on the competition between sediment supply and erosion (Figures 5 and S1). Topography in the minimal sedimentation regime can only be smoothed out substantially when sediment supply outcompetes minimal erosion effects. Surface offsets in the minimal sedimentation regime are typically as large as basement offsets (RMS heights for basement (120.6 m) versus seafloor (92.7 m)), and the flattening of seafloor curvature with time has a low slope (Figure 6). The topography in the minimal sedimentation regime is not entirely to the result of modern processes, however. Much of the track shown lies on Eocene crust, and equatorial sedimentation rates then were significantly lower than modern rates because of the extremely shallow CCD and low levels of carbonate burial [*Pälike et al.*, 2008].

[47] On these long profiles we also examined changes in seafloor topography due to preferential basin infill ("sediment focusing") by making the first-order comparison in the thickness of sediment layer at the topography highs and lows over all the topography crossed. We used traveltime images for our analyses assuming the constant velocity of 1480 m/s for the sediment packet thereby linearly translating the differences in traveltime as thickness of sediments. The approach slightly underestimates the basement topography because acoustic velocity increases with sediment depth. Since sediment cover is nearly as thick on hills as in valleys, the basement topography error is small, because it is the difference between the two estimated elevations. For example, in a basin filled with 500 ms TWTT of sediment versus 400 ms TWTT on the hill, the topographic height of the hill using an average sound velocity of 1480 m/s versus 1600 m/s is 6 m. The TWTT of our seismic interpretation is listed in Data Set S1, for those that want to apply a more complex model (TWTT data archived in Data Set S1).

[48] Using a constant acoustic velocity is also valid because we are simply calculating the relative thickness of the nearby sediment packets but not the time evolution of the sediment packets. To remove any directional biases, we took both eastward and westward combinations of topography highs and lows to calculate the ratio of the sediment thickness of topography low to high (hereafter "transport factors," i.e., implied transport from abyssal high to the basin). A transport factor higher than 1 indicates that more sediments accumulated in the topographic low than on the high and indicates that there is sediment focusing in the basin.

[49] Overall, the resulting transport factors are similar regardless of sedimentation regimes. Although the mean value marks its highest and lowest in the depositional and minimal sedimentation regimes, respectively, they are only 17% difference. On average, the sediment thicknesses on the topographic highs and lows are similar, with some slight excess in the topographic lows. The largest relative infill is no more than a factor of 2 (green and purple circles in Figure 5 or see Table 4), and only occurs 4 times out of 166 hill-basin combinations. The observations on the transect profiles also show that the seafloor flattening process is not strongly correlated to different sedimentation regimes and infers that sediment deposition is not excessively focused into the basins. Instead, low sedimentation mostly affects the distribution of the younger sediment package.

5. Discussion: Is Sediment Focusing Occurring in the Equatorial Pacific?

[50] Our study examines seismic reflection profiles from over 6000 km of the eastern equatorial Pacific. This large-scale reconnaissance provides significant insights into the sedimentation and sediment transport regimes occurring in the Pacific pelagic setting. The most important, though not unexpected, observation is that the region can be divided into different sedimentation regimes based on average sedimentation rate. Another finding is that syndepositional sediment transport from abyssal hills to valleys is relatively small. This observation is in contrast to geochemical estimates based on ^{230}Th, and which have been proposed to normalize sediment fluxes for paleoceanographic studies [*Francois et al.*, 2004].

[51] In certain depositional environments sediment focusing is a major factor causing large changes in

Table 4. A Summary of the Ratio of Sediment Thickness on the Topography Highs and Lows[a]

Line A (jd80: Depositional)		Line B (jd91: Transitional)		Line C (jd93: Minimal)	
E-W Comb.	W-E Comb.	E-W Comb.	W-E Comb.	E-W Comb.	W-E Comb.
1.00	1.40	1.00	1.33	1.00	1.13
1.38	1.20	1.33	1.25	1.17	1.00
1.22	1.00	1.00	1.67	0.83	1.29
1.50	1.17	1.14	0.75	1.00	1.29
1.38	1.17	1.00	1.33	1.20	1.00
1.00	1.17	1.14	1.67	1.40	1.00
1.43	1.67	1.33	1.14	0.83	1.40
1.22	2.00	1.33	1.14	1.00	1.20
1.43	1.43	2.00	1.00	1.50	1.17
1.25	1.50	1.00	1.00	1.33	1.17
0.14	1.80	1.00	1.33	1.00	1.17
1.14	1.67	1.00	1.00	1.33	0.83
1.00	1.00	1.00	1.67	1.14	1.14
1.67	1.14	1.00	1.67	1.17	1.33
1.60	1.43	1.33	1.00	1.00	0.83
1.50	1.25	1.14	1.14	1.33	1.33
1.29	1.43	1.00	1.33	0.83	1.00
2.00	1.22	1.33	1.00	1.33	1.14
1.67	1.43	1.67	1.00	1.17	1.33
1.67	1.00	1.25	1.00	1.17	1.00
1.17	1.38	1.33	1.00	1.17	1.33
1.17	1.50	1.00	2.00	1.20	1.50
1.33	1.22	1.00	1.33	1.40	1.00
1.17	1.38	1.00	1.14	1.00	1.17
1.20	1.00	1.14	1.00	1.00	1.00
1.20	1.14	1.14	1.29	0.83	
		1.00	1.29	1.40	
		1.33	1.00	1.00	
		1.00	1.13	0.83	
			1.17		
			1.00		
1.30[b]	1.34[b]	1.18[b]	1.23[b]	1.15[b]	1.14[b]

[a]Values indicate the basin flattering factor calculated from the thickness of sediments in topography low/high in a basin. E-W comb. and W-E comb. indicate eastward (from left to right on the profiles in Figure 5) and westward (from right to left on the profiles in Figure 5) combinations of topography highs and lows.
[b]Mean value.

sediment accumulation rates over short length scales (e.g., terrestrial environments as in the works by *Likens and Davis* [1975], *Lehman* [1975], and *Blais and Kalff* [1995] and oceanic environment as in the works by *Faugères et al.* [1999] and *Stow et al.* [2002]). In the eastern equatorial Pacific we do not observe such differences, and must ask to what extent are sedimentation processes of the equatorial Pacific unique?

[52] The sediments of the tropical Pacific are essentially all biogenic in origin [*Pälike et al.*, 2010] and are subject to dissolution before later burial. Unlike clay sediments, not all the sediments eroded are redeposited elsewhere; the disappearance of sediments via dissolution is not negligible. Biogenic silica is everywhere undersaturated and will dissolve at any location where it is not buried rapidly. $CaCO_3$ also has significant dissolution below the lysocline until it all disappears below the CCD. The late Pleistocene lysocline in the eastern tropical Pacific west of the East Pacific Rise is about 3.5 km [*Lyle et al.*, 1995], so carbonates are being dissolved at the seafloor on all the profiles. Sediment that is buried represents the net difference between carbonate production and loss via depth-dependent changes in dissolution rate [*Boudreau et al.*, 2010]. Sediment is not simply being transported from abyssal hills to abyssal basins. Instead, much of the sediment disappears in the process of transport and reburial due to dissolution, especially in the minimal sediment regime. In the equatorial Pacific where the sedimentation rates drastically change with respect to the high-productivity zone, it is important to recognize that these erosion and dissolution processes leave an imprint when the sediment is horizontally transported.

[53] There has been a debate for more than a decade about the extent of sediment focusing into topographic lows in the equatorial Pacific [e.g., *Francois et al.*, 2004; *Lyle et al.*, 2005]. The debate is essentially based on different results derived from two different approaches to calculating sediment mass accumulation rates: (1) by using geochemically derived sediment flux (e.g., *Francois et al.* [2004] and many works by other investigator) and (2) by using the mass of sediment that has accumulated between dated sediment horizons (e.g., *Lyle and Dymond* [1976] and many works by other investigators).

[54] *Francois et al.* [2004] pointed out that the mass accumulation rate approach neglects variations in particle flux rates between time A and time B. They suggested an alternative approach using a constant flux tracer. They proposed that the mass accumulation rate of sediments could be calculated using ^{230}Th-normalized sediment flux model [see also *Bacon*, 1984]. This model assumes the constant flux of ^{230}Th, and so vertical fluxes originating from the water column can be calculated by normalizing ^{230}Th measured in the sediment to the model production in the overlying water column (detailed method and rationale are given by *Francois et al.* [2004, section 3]).

[55] Using the ^{230}Th normalization method, *Francois et al.* [1990] defined a sediment focusing factor between a given time interval as the concentration of ^{230}Th in the sediment times the bulk dry density of the sediment within that interval. Sediment focusing factors >1 imply a higher flux of ^{230}Th from the water column than that expected by surface production; thus, they interpreted such excess of ^{230}Th to represent the flux of laterally advected particles. *Higgins et al.* [1999], *Marcantonio et al.* [2001], and *Loubere et al.* [2004] calculated sediment focusing factors in the equatorial Pacific and showed that in the equatorial Pacific much of the region has focusing factors >1, indicative of higher particle flux into particular locales by lateral advection by deep ocean currents. In some cases, sediment focusing factors >8 have been calculated [e.g., *Loubere et al.*, 2004], implying that significant syndepositional sediment transportation on the seafloor occurred [e.g., *Francois et al.*, 2004]. *Lyle et al.* [2005, 2007] used geologic evidence to argue that such high levels of sediment focusing predicted from the focusing factor calculated with ^{230}Th normalization method probably did not occur. Further investigations are needed to resolve this debate, including the analyses of near-bottom water chemistry, better understanding of water column particle flux, and measurements of ^{230}Th and stratigraphy using same core and seismic data. Nevertheless, our study here provides a significant line of evidence on the syndepositional sediment redistribution that can constrain the origin of sediment focusing events predicted by focusing factors.

[56] Our observations of topography smoothing and basin flattening processes from seismic profiles show that the sediment thickness between topography high and nearby low do not typically exceed more than a factor of 2 and the average of 1.3 in the depositional regime, and ~1.15–1.2 in the transitional and minimal sediment regimes (Table 4 and Figure S1). This means that the degree of sediment focusing suggested from ^{230}Th normalized mass accumulation rates may not be due to the syndepositional sediment redistribution. This hypothesis can be tested by a simple sediment redistribution model.

[57] We assume that sediment is being redistributed by an advecting near-seafloor current, as *Francois et al.* [2004] propose in order not to fractionate ^{230}Th in the transported sediment. The mechanisms to suspend sediments and transport them to a site of interest at the bottom of ocean with topography are poorly known. One of the most feasible drivers may be internal waves that are generated by a current advecting over bottom topography ("lee wave" in the works by *Bell* [1975] and *Garrett and Munk* [1979]), the effect of such internal waves may vary locally due to the balance between tidal energy and topographic complication [e.g., *St. Laurent and Garrett*, 2002]. On the other hand, such internal waves are rather common in shallow level in the modern oceans. Because it is not our intention to determine the origin of kinetic energy that transports sediments here, we accept this assumption as consistent to our model.

[58] Based on this assumption, we set up a simple model to describe the case that the even redistribution of sediments (the simplest case) by erosion when syndepositional sediment redistribution occurs, all the sediment eroded from the topographic high is deposited into the topographic low without compaction or dissolution. We set a hypothetical combination of topography high (TH) and low (TL) (Figure 9) with an arbitrary scale in the lateral direction, a 100 m of difference in the basement topography, and the initial conditions of sediment thickness of IS (Figure 9). This model assumes equal area of abyssal hills and basins. In

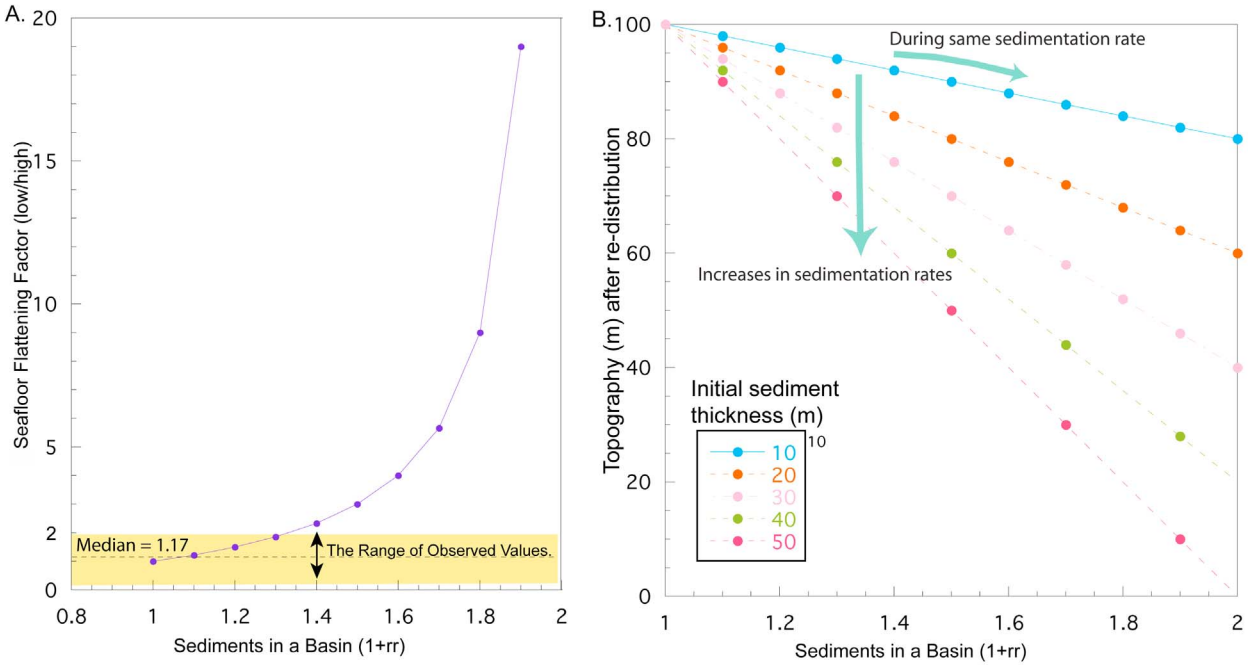

Figure 9. (a) The curve showing the basin flattening in a basin. The dotted line shows the level of our observations in this study (see Figure 4 and section 4.5). (b) A simple model of sediment redistribution (see detailed description in section 5).

nature, our TH and TL should indicate the archetypical abyssal-hill-scale peaks and troughs. The fraction of the redistributed sediment is indicated by *rr* in thickness ($0 \leq rr < 1$). We define the aforementioned seafloor flattening, or sediment transport factor (TF) as a sole function of the fraction (percentage) of redistribution,

$$TF = \frac{low}{high} = \frac{1 + rr}{1 - rr}$$

The value TF is the ratio in thickness of sediments on topographic highs and lows that we observed on the transect profile in section 4.5 (Figure S1). How much topography is subdued by such sediment redistribution, SF, is hence expressed as

$$SF = topography\_after\_redistribution$$

$$= (TH + IS^{*}(1 - rr)) - (TL + IS^{*}(1 + rr))$$

The term 1 + *rr* is equivalent to a long-term sediment focusing factor within the basins. With these initial conditions and formulations, we drew the relationship between (1) seafloor flattening (TF) and sediment focusing factor (1 + rr) and (2) the sediment focusing factor and the seafloor topography after the redistribution in the cases of initial sediment thickness (IS) from 10 to 50 m on the 100 m topographic difference to evaluate to what extent we may observe sediment focusing into basins from our seismic profiles (Figure 9). The resulting diagram shows that the progress of the sediment redistribution occurring under the same sedimentation rates follows each curve along the *x* axis direction, while the increase in sediment thickness by different sedimentation rates follows curves along the *y* axis direction. When the seafloor moves across the different sedimentation regimes from a depositional regime to the transitional or minimal sedimentation regime, the synthetic curves are drawn indicating the progress of the sediment redistribution through the different sedimentation regimes over time (thick blue arrows in Figure 9b).

[59] We applied this simple model to our observations on the transect profile to evaluate sediment focusing. The seafloor flattening between the topographic high and low in the depositional regime average 1.3 and range between 1.0 and 2.0 in the depositional transect profile, for example (see section 4.5). Using the TF relationship, we derive an average focusing factor (Figure 9a, equivalent to what should be the Th^{230} focusing factor) of 1.1 and a range between 1 and 1.3. Furthermore, with the most extreme case, we still observe that the sediment focusing occurs at much smaller scales than that predicted from the Th^{230} normalization method; even when all sediment is

redistributed from the topographic high to the low without any loss, sediment focusing into the basin (above (1 + rr)) occurs with only a factor of 2 (red marker in Figure 9b).

[60] The dynamics of large-scale resuspended sediment transport in the deep Pacific Ocean is poorly known. Nevertheless, seismic horizons in the tropical Pacific can be traced over >1000 km so there is little evidence of large-scale sediment redistribution obliterating the seismic continuity above the CCD. Instead we observe minor focusing from abyssal hills to abyssal basins as part of ongoing sedimentation processes, probably occurring at or very near the time of original sediment deposition. Occasionally we observe local sedimentation events that affect individual basins or hill regions, e.g., concentrated erosion or slump deposits. Asymmetric and discontinuous deposition of clays in the minimal sedimentation areas suggests that there is horizontal sediment transport and that it most strongly affects the fine fraction. Unlike terrestrial erosion and transportation of sediments, reworked sediments in the deep Pacific Ocean do not conserve mass during transport and initial redeposition. The ultimate preservation of resuspended sediments probably depends on many parameters including changes in the bottom water chemistry, the dissolution of sedimentary constituents and the kinetics of particles [e.g., *Edmond*, 1974; *Broecker*, 1971; *Dymond and Lyle*, 1985]. Although further investigation to understand the dynamics of this process is necessary, from our first-order observation and analyses on the equatorial Pacific sediment records, we suggest that "sediment focusing" is not the most important process to explain sediment distribution in either time or space in the equatorial Pacific seafloor.

6. Conclusions

[61] Broad-scale sedimentation in the equatorial Pacific can be divided into three distinct regimes: depositional, transitional, and minimal depositional regimes. These three sedimentation regimes host distinct basin-filling processes related to the average rate and consistency at which the sediments have accumulated through time.

[62] Sediment covered seafloor topography is slightly subdued relative to basement topography by preferential infilling of basins. The smoothing of topography depends on the thickness of overlying sediment blanket. Nevertheless, the sediment covered seafloor exhibits relief only slightly flatter than that of the buried ocean crust at all the study sites. The seafloor flattening process is not strongly correlated to the different sedimentation regimes. Basin sediment thickness is only 15%–30% thicker than that on hills, with the minimal sedimentation regime averaging 15% and the depositional regime averaging 30%. The largest difference in thickness between adjacent abyssal hills and basins was only a factor of 2, which translates into a focusing factor, assuming equivalent area of hills and basins, of 1.3. This is far smaller than ^{230}Th based focusing factors. From this observation, we suggest that "sediment focusing" is not one of the primary processes in either time or space shaping sedimentation in the pelagic equatorial Pacific.

[63] We also observed 3 generations of faults on the seismic profiles that could provide fluid pathways connecting the ocean and basaltic basement, and could define a CCD seismically at 4440 m on Pacific crust about 32 million years old.

Acknowledgments

[64] M. Lyle and N. C. Mitchell thank the captain and crew of R/V *Revelle* as well as shipboard geophysical service from Scripps Institution of Oceanography for the success of AMAT03 cruise. We thank Ted Moore, Larry Mayer, and John Goff for their helpful reviews that improved this manuscript. This research is supported by NSF grants OCE-07253011 and OCE-0851056 (M. Lyle and M. Tominaga) and NERC grant NE/C508985/2 (N. C. Mitchell).

References

Alldredge, A. L., and C. Gotschalk (1988), In situ settling behavior of marine snow, *Limnol. Oceanogr.*, *33*, 339–351, doi:10.4319/lo.1988.33.3.0339.

Arbic, B. K., J. F. Shriver, P. J. Hogan, H. E. Hurlburt, J. L. McClean, E. J. Metzger, R. B. Scott, A. Sen, O. M. Smedstad, and A. J. Wallcraft (2009), Estimates of bottom flows and bottom boundary layer dissipation of the oceanic general circulation from global high-resolution models, *J. Geophys. Res.*, *114*, C02024, doi:10.1029/2008JC005072.

Bacon, M. P. (1984), Glacial to interglacial changes in carbonate and clay sedimentation in the Atlantic ocean estimated from ^{230}Th measurements, *Isot. Geosci.*, *2*, 97–111.

Barron, J. A., E. Fourtanier, and S. M. Bohaty (2004), Oligocene and earliest Miocene diatom biostratigraphy of ODP Leg 199 Site 1220, equatorial Pacific [online], *Proc. Ocean Drill. Program Sci. Results*, *199*, 25 pp. (Available at http://www-odp.tamu.edu/publications/199_SR/204/204.htm)

Bekins, B. A., A. J. Spivack, E. E. Davis, and L. A. Mayer (2007), Dissolution of biogenic ooze over basement edifices in the equatorial Pacific with implications for hydrothermal ventilation of the oceanic crust, *Geology*, *35*, 679–682, doi:10.1130/G23797A.1.

Bell, T. H. (1975), Topographically generated internal waves in the open ocean, *J. Geophys. Res.*, *80*, 320–327, doi:10.1029/JC080i003p00320.

Berger, W. H., C. G. Adelseck, and L. A. Mayer (1976), Distribution of carbonate in surface sediments of the Pacific Ocean, *J. Geophys. Res.*, *81*, 2617–2627, doi:10.1029/JC081i015p02617.

Blais, J. M., and J. Kalff (1995), The influence of lake morphometry on sediment focusing, *Limnol. Oceanogr.*, *40*, 582–588, doi:10.4319/lo.1995.40.3.0582.

Bloomer, S. F., L. A. Mayer, and T. C. Moore Jr. (1995), Seismic stratigraphy of the eastern equatorial Pacific Ocean: Paleoceanographic implications, *Proc. Ocean Drill. Program Sci. Results*, *138*, 537–553. doi:10.2973/odp.proc.sr.138.128.1995.

Boudreau, B. P., J. J. Middleburg, and F. J. R. Meysman (2010), Carbonate compensation dynamics, *Geophys. Res. Lett.*, *37*, L03603, doi:10.1029/2009GL041847.

Broecker, W. S. (1971), A kinetic model for the chemical composition of sea water, *Quat. Res.*, *1*, 188–207, doi:10.1016/0033-5894(71)90041-X.

Bryant, W. R., and R. H. Bennet (1988), Origin, physical, and mineralogical nature of red clays: The Pacific Ocean basin as a model, *Geo Mar. Lett.*, *8*, 189–249, doi:10.1007/BF02281640.

Buck, W. R., L. L. Lavier, and A. N. B. Poliakov (2005), Modes of faulting at mid-ocean ridges, *Nature*, *434*, 719–723.

Culling, W. E. H. (1962), Analytical theory of erosion, *J. Geol.*, *68*, 336–344.

DeMets, C., R. G. Gordon, and D. F. Argus (2010), Geologically current plate motions, *Geophys. J. Int.*, *181*, 1–80, doi:10.1111/j.1365-246X.2009.04491.x.

Dymond, J., and M. Lyle (1985), Flux comparisons between sediments and sediment traps in the eastern tropical Pacific: Implications for atmospheric CO_2 variations during the Pleistocene, *Limnol. Oceanogr.*, *30*, 699–712, doi:10.4319/lo.1985.30.4.0699.

Edmond, J. M. (1974), On the dissolution of carbonate and silicate in the deep ocean, *Deep Sea Res.*, *21*, 455–480.

Engebretson, D. C., A. Cox, and R. G. Gordon (1984), Relative motions between oceanic plates of the Pacific basin, *J. Geophys. Res.*, *89*, 10,291–10,310, doi:10.1029/JB089iB12p10291.

Ewing, M., J. I. Ewing, and M. Talwani (1964), Sediment distribution in the oceans: The Mid-Atlantic Ridge, *Geol. Soc. Am. Bull.*, *75*, 17–36, doi:10.1130/0016-7606(1964)75[17:SDITOT]2.0.CO;2.

Ewing, J., J. L. Worzel, M. Ewing, and C. Windisch (1966), Ages of horizon A and the oldest Atlantic sediments, *Science*, *154*, 1125–1132, doi:10.1126/science.154.3753.1125.

Farrell, J. W., and W. L. Prell (1989), Climatic change and $CaCO_3$ preservation: An 800,000 year bathymetric reconstruction from the central equatorial Pacific Ocean, *Paleoceanography*, *4*, 447–466, doi:10.1029/PA004i004p00447.

Faugères, J.-C., D. A. V. Stow, P. Imbert, and A. Viana (1999), Seismic features diagnostic of contourite drifts, *Mar. Geol.*, *162*, 1–38, doi:10.1016/S0025-3227(99)00068-7.

Flood, R. D. (1988), A lee wave model for deep-sea mudwave activity, *Deep Sea Res.*, *35*, 973–983, doi:10.1016/0198-0149(88)90071-4.

Francois, R., M. P. Bacon, and D. O. Suman (1990), Thorium-230 profiling in deep-sea sediments: High-resolution records of flux and dissolution of carbonate in the equatorial Atlantic during the last 24,000 years, *Paleoceanography*, *5*(5), 761–787.

Francois, R., M. Frank, M. M. Rotgers van der Loeff, and M. P. Bacon (2004), ^{230}Th normalization: An essential tool for interpreting sedimentary fluxes during the late Quaternary, *Paleoceanography*, *19*, PA1018, doi:10.1029/2003PA000939.

Francois, R., et al. (2007), Comment on "Do geochemical estimates of sediment focusing pass the sediment test in the equatorial Pacific?" by M. Lyle et al., *Paleoceanography*, *22*, PA1216, doi:10.1029/2005PA001235.

Garrett, C., and W. Munk (1979), Internal waves in the ocean, *Annu. Rev. Fluid Mech.*, *11*, 339–369, doi:10.1146/annurev.fl.11.010179.002011.

Goff, J. A. (1991), A global and regional stochastic analysis of near-ridge abyssal hill morphology, *J. Geophys. Res.*, *96*, 21,713–21,737, doi:10.1029/91JB02275.

Goff, J. A., and T. H. Jordan (1988), Stochastic modeling of seafloor morphology: Inversion of Sea Beam data for second-order statistics, *J. Geophys. Res.*, *93*, 13,589–13,608.

Goff, J. A., and T. H. Jordan (1990), Pacific and Atlantic models of small-scale seafloor topography, *Rep. on Acoust. Reverberation Tech. Rep., 1*, Off. of Nav. Res., Arlington, Va.

Gripp, A. E., and R. G. Gordon (1990), Current plate velocities relative to the hotspots incorporating the NUVEL-1 global plate motion model, *Geophys. Res. Lett.*, *17*, 1109–1112, doi:10.1029/GL017i008p01109.

Heezen, B. C., and M. Rawson (1977), Visual observations of contemporary current erosion and tectonic deformation on the Cocos Ridge crest, *Mar. Geol.*, *23*, 173–196, doi:10.1016/0025-3227(77)90088-3.

Higgins, S. M., W. S. Broecker, R. F. Anderson, D. C. McCorkle, and D. Timothy (1999), Enhanced sedimentation along the equator in the western Pacific, *Geophys. Res. Lett.*, *26*, 3489–3492.

Honjo, S., J. Dymond, R. Collier, and S. J. Manganini (1995), Export production of particles to the interior of the equatorial Pacific Ocean during the 1992 EqPac experiment, *Deep Sea Res.*, *42*, 831–870, doi:10.1016/0967-0645(95)00034-N.

Jordan, T. H., W. Menard, and D. K. Smith (1983), Density and size distribution of seamounts in the eastern Pacific inferred from wide-beam sounding data, *J. Geophys. Res.*, *88*, 10,508–10,518, doi:10.1029/JB088iB12p10508.

Koppers, A. A. P., J. Phipps Morgan, W. J. Morgan, and H. Staudigel (2001), Testing the fixed hotspot hypothesis using ^{40}Ar/^{39}Ar age progressions along seamount trails, *Earth Planet. Sci. Lett.*, *185*, 237–252, doi:10.1016/S0012-821X(00)00387-3.

Korenaga, J. (2007), Thermal cracking and the deep hydration of oceanic lithosphere: A key to the generation of plate tectonics?, *J. Geophys. Res.*, *112*, B05408, doi:10.1029/2006JB004502.

Kriner, K. A., R. A. Pockalny, and R. L. Larson (2006), Bathymetric gradients of lineated abyssal hills: Inferring seafloor spreading vectors and a new model for hills formed at ultra-fast rates, *Earth Planet. Sci. Lett.*, *242*, 98–110.

Laguros, G. A., and T. H. Shipley (1989), Quantitative estimate of resedimentation in the pelagic sequence of the equatorial Pacific, *Mar. Geol.*, *89*, 269–277.

Lancelot, Y., and R. L. Larson (1975), Sedimentary and tectonic evolution of northwestern Pacific, *Initial Rep. Deep Sea Drill. Proj.*, *XXXII*, 925–939, doi:10.2973/dsdp.proc.32.138.1975.

Lee, S.-M., and S. C. Solomon (1995), Constraints from Sea Beam bathymetry on the development of normal faults on the East Pacific Rise, *Geophys. Res. Lett.*, *22*, 3135–3138.

Lehman, J. T. (1975), reconstructing the rate of accumulation of lake sediment: The effect of sediment focusing, *Quat. Res.*, *5*, 541–550, doi:10.1016/0033-5894(75)90015-0.

Likens, G. E., and M. B. Davis (1975), Post-glacial history of Mirror Lake and its watershed in New Hampshire, U.S.A.: An initial report, *Verh. Int. Ver. Theor. Angew. Limnol.*, *19*, 982–993.

Lister, C. R. B. (1976), Control of pelagic sediment distributions by internal waves of tidal period: Possible interpretation of data from the southern East Pacific Rise, *Mar. Geol.*, *20*, 297–313, doi:10.1016/0025-3227(76)90109-2.

Lonsdale, P., and S. M. Smith (1980), "Lower insular rise hills" shaped by a bottom boundary current in the mid-Pacific, *Mar. Geol.*, *34*, M19–M25, doi:10.1016/0025-3227(80)90133-4.

Loubere, P., F. Mekik, R. Francois, and S. Pichat (2004), Export fluxes of calcite in the eastern equatorial Pacific from the Last Glacial Maximum to present, *Paleoceanography*, *19*, PA2018, doi:10.1029/2003PA000986.

Lyle, M. (2003), Neogene carbonate burial in the Pacific Ocean, *Paleoceanography*, *18*(3), 1059, doi:10.1029/2002PA000777.

Lyle, M. W., and J. Dymond (1976), Metal accumulation rates in the southeast Pacific—Errors introduced from assumed bulk densities, *Earth Planet. Sci. Lett.*, *30*, 164–168, doi:10.1016/0012-821X(76)90242-9.

Lyle, M., K. A. Dadey, and J. W. Farrell (1995), The late Miocene (11–8 Ma) eastern Pacific carbonate crash: Evidence for reorganization of deep-water circulation by the closure of the Panama Gateway, *Proc. Ocean Drill. Program Sci. Results*, *138*, 821–838, doi:10.2973/odp.proc.sr.138.157.1995.

Lyle, M., et al. (2002a), Proceedings of the Ocean Drilling Program, Initial Reports, vol. 199, doi:10.2973/odp.proc.ir.199.2002, Ocean Drill. Program, College Station, Tex.

Lyle, M., L. Liberty, T. C. Moore Jr., and D. K. Rea (2002b), Development of a seismic stratigraphy for the Paleogene sedimentary section, central tropical Pacific Ocean, *Proc. Ocean Drill. Program Initial Rep.*, *199*, 1–21, doi:10.2973/odp.proc.ir.199.104.2002.

Lyle, M., N. Mitchell, N. Pisias, A. Mix, J. I. Martinez, and A. Payton (2005), Do geochemical estimates of sediment focusing pass the sediment test in the equatorial Pacific?, *Paleoceanography*, *20*, PA1005, doi:10.1029/2004PA001019.

Lyle, M., N. Pisias, A. Paytan, J. I. Martinez, and A. Mix (2007), Reply to comment by R. Francois et al. on "Do geochemical estimates of sediment focusing pass the sediment test in the equatorial Pacific?": Further explorations of ^{230}Th normalization, *Paleoceanography*, *22*, PA1217, doi:10.1029/2006PA001373.

Lyle, M., H. Pälike, H. Nishi, I. Raffi, K. Gamage, A. Klaus, and the IODP Expeditions 320/321 Scientific Party (2010), The Pacific Equatorial Age Transect, IODP Expeditions 320 and 321: Building a 50-million-year-long environmental record of the equatorial Pacific Ocean, *Sci. Drill.*, *9*, 4–15, doi:10.2240/iodp.sd.9.01.2010.

Macdonald, K. C., P. J. Fox, R. T. Alexander, R. Pockalny, and P. Gente (1996), Volcanic growth faults and the origin of Pacific abyssal hills, *Nature*, *380*, 125–129, doi:10.1038/380125a0.

Malinverno, A. (1990), A quantitative study of the axial topography of the Mid-Atlantic Ridge, *J. Geophys. Res.*, *95*, 2645–2660, doi:10.1029/JB095iB03p02645.

Marcantonio, F., R. F. Anderson, S. Higgins, M. Stute, P. Schlosser, and P. Kubik (2001), Sediment focusing in the central equatorial Pacific Ocean, *Paleoceanography*, *16*, 260–267, doi:10.1029/2000PA000540.

Mayer, L. A., T. H. Shipley, F. Theyer, R. H. Wilkens, and E. L. Winterer (1985), Seismic modeling and paleoceanography at deep sea drilling project Site 574, *Deep Sea Drill. Proj.*, *85*, 947–970.

Mayer, L. A., T. H. Shipley, and E. L. Winterer (1986), Equatorial Pacific seismic reflectors as indicators of global oceanographic events, *Science*, *233*, 761–764, doi:10.1126/science.233.4765.761.

McCarthy, M. C., S. E. Kruse, M. R. Brudzinski, and M. E. Ranieri (1996), Changes in plate motions and the shape of Pacific fracture zones, *J. Geophys. Res.*, *101*, 13,715–13,730, doi:10.1029/96JB00646.

McCave, I. N. (1975), Vertical flux of particles in the ocean, *Deep Sea Res.*, *22*, 491–502.

McCave, I. N. (1984), Erosion, transport and deposition of fine-grained marine sediments, in *Fine-Grained Sediments: Deep Water Processes and Facies*, edited by D. A. V. Stow and D. J. W. Piper, *Geol. Soc. Spec. Publ.*, 15, 35–69.

McManus, J. F., D. W. Oppo, and J. L. Cullen (1999), A 0.5-million-year record of millennial-scale climate variability in the North Atlantic, *Science*, *283*, 971–975, doi:10.1126/science.283.5404.971.

Meadows, A., and P. S. Meadows (1994), Bioturbation in deep sea Pacific sediments, *J. Geol. Soc.*, *151*, 361–375.

Menard, H. W. (1964), *Marine Geology of the Pacific*, 271 pp., McGraw-Hill, New York.

Menard, H. W., and J. Mammerickx (1967), Abyssal hills, magnetic anomalies and the east pacific rise, *Earth Planet. Sci. Lett.*, *2*, 465–472, doi:10.1016/0012-821X(67)90191-4.

Mitchell, N. C. (1995), Diffusion transport model for pelagic sediments on the Mid- Atlantic Ridge, *J. Geophys. Res.*, *100*, 19,991–20,009, doi:10.1029/95JB01974.

Mitchell, N. C. (1998), Modeling Cenozoic sedimentation in the central equatorial Pacific and implications for true polar wander, *J. Geophys. Res.*, *103*, 17,749–17,766.

Mitchell, N. C., and J. M. Huthnance (2007), Comparing the smooth, parabolic shapes of interfluves in continental slopes to predictions of diffusion transport models, *Mar. Geol.*, *236*, 189–208, doi:10.1016/j.margeo.2006.10.028.

Mitchell, N. C., M. W. Lyle, M. B. Knappenberger, and L. M. Liberty (2003), Lower Miocene to present stratigraphy of the equatorial Pacific sediment bulge and carbonate dissolution anomalies, *Paleoceanography*, *18*(2), 1038, doi:10.1029/2002PA000828.

Moore, T. C., Jr., J. Backman, I. Raffi, C. Nigrini, A. Sanfilippo, H. Pälike, and M. Lyle (2004), Paleogene tropical Pacific: Clues to circulation, productivity, and plate motion, *Paleoceanography*, *19*, PA3013, doi:10.1029/2003PA000998.

Moore, T. C., Jr., N. C. Mitchell, M. Lyle, J. Backman, and H. Pälike (2007), Hydrothermal pits in the biogenic sediments of the equatorial Pacific Ocean, *Geochem. Geophys. Geosyst.*, *8*, Q03015, doi:10.1029/2006GC001501.

Müller, R. D., M. Sdrolias, C. Gaina, and W. R. Roest (2008), Age, spreading rates, and spreading asymmetry of the world's ocean crust, *Geochem. Geophys. Geosyst.*, *9*, Q04006, doi:10.1029/2007GC001743.

Nigrini, C., A. Sanfilippo, and T. J. Moore Jr. (2006), Cenozoic radiolarian biostratigraphy: A magnetobiostratigraphic chronology of Cenozoic sequences from ODP Sites 1218, 1219, and 1220, equatorial Pacific, *Proc. Ocean Drill. Program Sci. Results*, *199*, 1–76, doi:10.2973/odp.proc.sr.199.225.2006.

Pälike, H., T. Moore, J. Backman, I. Raffi, L. Lanci, J. M. Parés, and T. Janecek (2005), Integrated stratigraphic correlation and improved composite depth scales for ODP Sites 1218 and 1219, *Proc. Ocean Drill. Program Sci. Results*, *199*, 1–41, doi:10.2973/odp.proc.sr.199.213.2005.

Pälike, H., M. W. Lyle, N. Ahagon, I. Raffi, K. Gamage, and C. A. Zarikian (2008), Pacific equatorial age transect [online], *Integrated Ocean Drill. Program Sci. Prospectus*, *320/321*, 96 pp., doi:10.2204/iodp.sp.320321.2008. (Available at http://publications.iodp.org/scientific_prospectus/320_321/index.html)

Pälike, H., H. Nishi, M. Lyle, I. Raffi, A. Klaus, K. Gamage, and the Expedition 320/321 Scientists (2009), Pacific equatorial transect [online], *Integrated Ocean Drill. Program Prelim. Rep.*, *320*, 175 pp., doi:10.2204/iodp.pr.320.2009. (Available at http://publications.iodp.org/preliminary_report/320/)

Pälike, H., M. Lyle, H. Nishi, I. Raffi, K. Gamage, A. Klaus, and the Expedition 320/321 Scientists (2010), Proceedings of the Integrated Ocean Drilling Program, vol. 320/321, doi:10.2204/iodp.proc.320321.101.2010, Integrated Ocean Drill. Program, College Station, Tex.

Peterson, L. C., G. H. Haug, R. W. Murray, K. M. Yarincik, J. W. King, T. J. Bralower, K. Kameo, S. D. Rutherford, and R. B. Pearce (2000), Late Quaternary stratigraphy and sedimentation at Site 1002, Cariaco Basin (Venezuela), *Proc. Ocean Drill. Program Sci. Results*, *165*, 85–99, doi:10.2973/odp.proc.sr.165.017.2000.

Pisias, N. G., L. A. Mayer, T. R. Janecek, A. Palmer-Julson, and T. H. van Andel (1995), *Proceedings of the Ocean Drilling Program: Scientific Results*, vol. 138, Ocean Drill. Program, College Station, Tex.

Rea, D. K., and M. W. Lyle (2005), Paleogene calcite compensation depth in the eastern subtropical Pacific: Answers and questions, *Paleoceanography*, *20*, PA1012, doi:10.1029/2004PA001064.

Roberts, D. G., N. G. Hogg, D. G. Bishop, and C. G. Flewellen (1974), Sediment distribution around moated seamounts in the Rockall Trough, *Deep Sea Res.*, *21*, 175–184.

Ryan, W. B. F., et al. (2009), Global Multi-Resolution Topography synthesis, *Geochem. Geophys. Geosyst.*, *10*, Q03014, doi:10.1029/2008GC002332.

Sager, W. W., and M. S. Pringle (1988), Mid-Cretaceous to Early Tertiary apparent polar wander path of the Pacific Plate, *J. Geophys. Res.*, *93*, 11,753–11,771, doi:10.1029/JB093iB10p11753.

Sandwell, D., and Y. Fialko (2004), Warping and cracking of the Pacific plate by thermal contraction, *J. Geophys. Res.*, *109*, B10411, doi:10.1029/2004JB003091.

Sandwell, D., and G. Schubert (1982), Lithospheric flexure at fracture zones, *J. Geophys. Res.*, *87*, 4657–4667, doi:10.1029/JB087iB06p04657.

Sen, A., R. B. Scott, and B. K. Arbic (2008), Global energy dissipation rate of deep-ocean low-frequency flows by quadratic bottom boundary layer drag: Computations from current-meter data, *Geophys. Res. Lett.*, *35*, L09606, doi:10.1029/2008GL033407.

Shipboard Scientific Party (2002), Leg 199 summary, *Proc. Ocean Drill. Program Initial Rep.*, *199*, 1–87, doi:10.2973/odp.proc.ir.199.101.2002.

Small, C. (1994), A global analysis of mid-ocean ridge axial topography, *Geophys. J. Int.*, *116*, 64–84, doi:10.1111/j.1365-246X.1994.tb02128.x.

Smith, D. K., and T. H. Jordan (1988), Seamount statistics in the Pacific Ocean, *J. Geophys. Res.*, *93*, 2899–2918, doi:10.1029/JB093iB04p02899.

St. Laurent, L., and C. Garrett (2002), The role of internal tides in mixing the deep ocean, *J. Phys. Oceanogr.*, *32*, 2882–2899, doi:10.1175/1520-0485(2002)032<2882:TROITI>2.0.CO;2.

Stow, D. A. V., J.-C. Faugeres, J. A. Howe, C. J. Pudsey, and A. Viana (2002), Bottom currents, contourites and deep-sea sediment drifts: Current state-of-the-art, in *Deep-Water Contourite Systems: Modern Drifts and Ancient Series, Seismic and Sedimentary Characteristics*, edited by D. A. V. Stow et al., *Geol. Soc. Mem.*, 22, 7–20.

Takahashi, K., and S. Honjo (1981), Vertical flux of radiolaria: A taxon-quantitative sediment trap study from the western tropical Atlantic, *Micropaleontology*, *27*, 140–190, doi:10.2307/1485284.

van Andel, T. H. (1975), Mesozoic/Cenozoic calcite compensation depth and the global distribution of calcareous sediments, *Earth Planet. Sci. Lett.*, *26*, 187–194, doi:10.1016/0012-821X(75)90086-2.

van Andel, T. H., and T. C. Moore (1974), Cenozoic migration of the Pacific plate, northward shift of the axis of deposition, and paleobathymetry of the central equatorial Pacific, *Geology*, *2*, 507–510, doi:10.1130/0091-7613(1974)2<507:CMOTPP>2.0.CO;2.

Webb, H. F., and T. H. Jordan (1993), Quantifying the distribution ad transport of pelagic sediments on young abyssal hills, *Geophys. Res. Lett.*, *20*, 2203–2206, doi:10.1029/93GL01881.

Webb, H. F., and T. H. Jordan (2001a), Pelagic sedimentation on rough seafloor topography 1. Forward model, *J. Geophys. Res.*, *106*, 30,433–30,449, doi:10.1029/2000JB900275.

Webb, H. F., and T. H. Jordan (2001b), Pelagic sedimentation on rough seafloor topography: 2. Inversion results from the north Atlantic acoustic reverberation corridor, *J. Geophys. Res.*, *106*, 30,451–30,473, doi:10.1029/2000JB900274.

Wilcock, W. S. D., G. M. Purdy, S. C. Solomon, D. L. Dubois, and D. R. Toomey (1992), Microearthquakes on and near the East Pacific Rise, 9°–10°N, *Geophys. Res. Lett.*, *19*, 2131–2134, doi:10.1029/92GL02208.

Wilkens, H., and T. Handyside (1985), Physical properties of equatorial Pacific sediments, *Initial Rep. Deep Sea Drill. Proj.*, *85*, 839–847.